Effects of Reaction Temperature and Support Composition on the Mechanism of WaterÀGas Shift Reaction over Supported-Pt Catalysts

ARTICLE *in* THE JOURNAL OF PHYSICAL CHEMISTRY C · MAY 2011

Impact Factor: 4.77 · DOI: 10.1021/jp201773a

5 AUTHORS, INCLUDING:

Christos M. Kalamaras
Saudi Arabian Oil Company
11 PUBLICATIONS **391** CITATIONS
SEE PROFILE

Angelos M Efstathiou
University of Cyprus
137 PUBLICATIONS **3,328** CITATIONS
SEE PROFILE

THE JOURNAL OF PHYSICAL CHEMISTRY C

ARTICLE

pubs.acs.org/JPCC

Effects of Reaction Temperature and Support Composition on the Mechanism of Water−Gas Shift Reaction over Supported-Pt Catalysts

Christos M. Kalamaras,[†] Ines D. Gonzalez,[‡] Rufino M. Navarro,[‡] José Luis G. Fierro,[‡] and Angelos M. Efstathiou*[,†]

[†]Department of Chemistry, Heterogeneous Catalysis Laboratory, University of Cyprus, University Campus, P.O. Box 20537, CY 1678, Nicosia, Cyprus

[‡]Instituto de Catalisis y Petroleoquímica (CSIC), Cantoblanco, 28049 Madrid, Spain

ABSTRACT: The present work reports on a detailed study of the effect of support chemical composition and reaction temperature on the mechanism of the water−gas shift (WGS) reaction over supported-Pt catalysts. The effect of the same parameters on the chemical composition and surface concentration of *active* reaction intermediates was also determined for the first time, information that allowed elucidating also the site location of these intermediates, e.g., support versus metal or support−metal interface. The above-mentioned mechanistic information was rigorously provided by the application of steady-state isotopic transient kinetic analysis (SSTIKA) experiments coupled with mass spectrometry (MS) and DRIFTS techniques, and by other transient isotopic experiments designed. It was found that on Pt/CeO_2 a switch of the WGS reaction mechanism from "redox" to a combination of redox and "associative formate with −OH group regeneration" is obtained after increasing the reaction temperature from 473 to 573 K. On the other hand, only the redox mechanism operates on Pt/TiO_2 of similar Pt mean particle size. Modification of titania support by the deposition of small crystallites of ceria in its pore structure enhanced significantly the activity of WGS at $T > 573$ K compared to Pt/TiO_2, whereas the operated mechanism resembles that occurring on Pt/CeO_2. In all supported-Pt catalysts investigated, the concentration of active "carbon-containing" intermediates found in the "carbon-path" was significantly lower than that found for the "hydrogen-containing" intermediates present in the "hydrogen-path", the latter being labile OH and H species formed on the support, and which were found to depend on the support chemical composition and reaction temperature. This study provides new important fundamental knowledge on the mechanism of WGS over practical supported metal catalysts which can be used for a better WGS catalyst design.

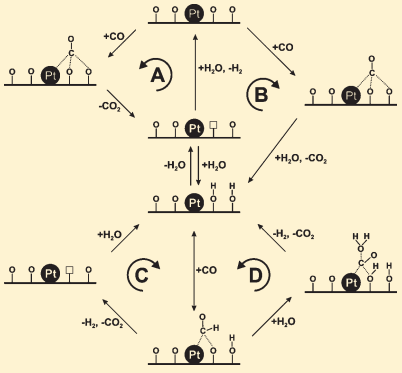

1. INTRODUCTION

The renewed interest in the water−gas shift (WGS) reaction ($CO + H_2O \leftrightarrow CO_2 + H_2$, $\Delta H^o = -41.1$ kJ/mol) has grown significantly during the last years as a result of recent advances in fuel cell technology and the need for developing fuel processors capable of converting carbonaceous fuels into hydrogen.[1−5] The role of the WGS reaction in these fuel processors is to reduce the content of CO in the reformate gas with simultaneous further hydrogen production. Fe_3O_4/Cr_2O_3 catalysts are used for the industrial production of hydrogen in the 593−723 K range to take advantage of the higher reaction rate at high temperatures (HT-WGS), whereas $Cu/ZnO/Al_2O_3$ catalysts are used in the 473−523 K range (LT-WGS) to take advantage of the higher hydrogen concentration at equilibrium.[5,6] These catalysts, however, are pyrophoric and deactivate if exposed to air and condensed water. Attempts are now focused toward the development of low-loading robust noble metal-based catalysts which are nonpyrophoric with high activity at low temperatures and resulting in a CO content of less than 10 ppm in hydrogen feed gas streams, when the latter are to be used in H_2 fuel cells.[4,7]

It is generally accepted that the WGS reaction over supported metal catalysts operates in a bifunctional manner with the participation of both the noble metal and the support. Two main WGS reaction pathways have been proposed in the literature[5,6] over reducible metal oxide supported metal catalysts: (i) the "*redox*" or regenerative mechanism, and (ii) the "*associative*" or adsorptive mechanism (nonredox). In the redox mechanism CO adsorbs on the noble metal surface which then diffuses at the metal/support interface and reacts with lattice oxygen of support to form CO_2(g), a step that results in the formation of oxygen vacant sites and thus reduction of support. Water adsorbs and dissociates mainly on the reduced support sites, thus reoxidizing them and producing H_2(g).[8−13] In the associative mechanism,[14−18] CO and H_2O are proposed to adsorb on catalyst active sites to form a surface "carbon-containing" intermediate, e.g., formate, carbonate, or bicarbonate, which further reacts or decomposes to form H_2 and CO_2. The chemical composition of this active carbon-containing intermediate and its true site location, e.g., support,

Received: February 23, 2011
Revised: May 1, 2011

   dx.doi.org/10.1021/jp201773a | *J. Phys. Chem. C* XXXX, XXX, 000–000

metal/support interface, or metal surface, still remain controversial issues.

There is an increasing demand for fundamental understanding at the molecular level of the LT-WGS reaction in order to achieve optimization of activity and stability under industrial conditions for the development of new suitable functional catalytic materials which will replace the existing ones that face several problems.[5,6] Recently, Zhai et al.[19] and previously Rodriguez et al.[20] have performed very thorough experimental and theoretical investigations to unravel the intrinsic reasons of the high activity exhibited by CeO_2- or TiO_2-supported Au and Pt nanoparticles toward the low-temperature WGS reaction. Both works found that stable and very active species along the periphery of the metal−support interface are formed during WGS reaction conditions, to mention Pt−O_x(OH)$_y$,[19] while oxygen vacancies along and close to this interface facilitate water dissociation, thus providing active −OH groups.[20] Furthermore, it was demonstrated[19] that the catalytic chemistry occurs on the atomically dispersed $Pt^{\delta+}$ or $Au^{\delta+}$ species; thus, the metal nanoparticles act merely as spectators during reaction. Thus, such findings become extremely important for the proper design of highly active and stable low-temperature WGS catalysts.

The steady-state isotopic transient kinetic analysis (SSITKA) technique coupled with DRIFTS and mass spectrometry (*operando*) is a powerful tool to investigate key mechanistic and kinetic aspects of the WGS reaction.[21−24] In particular, it is possible to probe the chemical composition, structure, and site location[22] of *active* reaction intermediates and of *inactive* (spectator) species found in the "carbon path" of the WGS reaction (e.g., adsorbed CO, formate, or carbonate), estimate the individual rate of the reaction path that involves each one of these intermediate species, and based on this information to decide on the importance of each one of these intermediates to the overall steady-state rate of WGS reaction. The surface concentration (μmol/g, θ (based on surface Pt)) of active "H-containing" (use of D_2O) and "C-containing" (use of ^{13}CO) reaction intermediates can also be measured by in situ SSITKA−mass spectrometry experiments,[21,22] and this important kinetic quantity allows for proper discussion of crucial mechanistic issues of the reaction at hand, such as the rate-determining step.

The aim of this work was to apply SSITKA−DRIFTS and SSITKA−mass spectrometry techniques to gather important fundamental information that would allow us to understand more deeply the effect of reaction temperature and support chemical composition on the mechanism of the heterogeneous WGS reaction on Pt/CeO_2, Pt/TiO_2, and Pt/CeO_2−TiO_2 catalysts in order to improve their formulation for optimum activity.

2. EXPERIMENTAL SECTION

2.1. Catalyst Preparation and Characterization. Cerium oxide (CeO_2) was prepared by coprecipitation of $(NH_4)_2Ce(NO_3)_6$ (Alfa-Aesar, 99.5%) and $La(NO_3)_3 \cdot 5H_2O$ (Alfa-Aesar, 99.9%) using urea $(NH_2)_2CO$ (Alfa-Aesar, 99.5%) as a precipitating agent.[25] The solid obtained was dried (383 K, 4 h) and then calcined in air (923 K, 8 h). The TiO_2 support (titanium(IV) oxide, Alfa Aesar, 150 m^2/g BET area) was stabilized by thermal treatment at 773 K for 4 h before being used for Pt deposition. The TiO_2 support modified with Ce (CeO_2−TiO_2, Ce/Ti atom ratio = 0.032) was synthesized by wet impregnation of titania powders (TiO_2, Alfa Aesar) with cerium nitrate aqueous solution. The final loading of ceria in the TiO_2 support was 6.6 wt %, which corresponds to 45% of surface monolayer coverage of TiO_2; a Ce/Ti atom ratio of 0.07 was reported to correspond to one surface monolayer.[26] The impregnated solid support was then calcined in air at 873 K for 8 h.

The corresponding supported-Pt catalysts (0.5 wt % Pt) were prepared by impregnating each of the supports with an aqueous solution of $H_2PtCl_6 \cdot xH_2O$ (Johnson-Mattey, 40.78 wt % Pt). After drying at 393 K overnight, the samples were calcined in air at 773 K for 3 h. The samples are designated Pt/TiO_2, Pt/CeO_2, and Pt/CeO_2−TiO_2 for platinum supported on titania, ceria, and ceria−titania, respectively.

The specific surface areas ($m^2 \cdot g^{-1}$) of the catalysts were estimated by applying the BET method. N_2 adsorption−desorption isotherms were obtained at 77 K over the entire range of relative pressures using the Micromeritics ASAP 2100 device on samples previously outgassed at 423 K for 12 h. Platinum dispersion was measured using a dynamic method described elsewhere.[27] Prior to H_2 chemisorption at 193 K, all samples were reduced under H_2/Ar flow (50 mL/min) for 1 h at 523 K and subsequently flushed in Ar flow for 15 min at 538 K. Metal dispersion was estimated after considering a hydrogen chemisorption stoichiometry of H/Pt = 1.[28] The crystal structure of the metal oxide supports prepared was checked by powder X-ray diffraction using a Seifert 3000P vertical diffractometer with a nickel-filtered CuKα radiation. For each sample, Bragg angles between 5 and 80° were scanned. Volume-averaged crystallite sizes were determined by applying the Debye−Scherrer equation.[29]

2.2. Catalytic Activity Measurements. Steady-state catalytic activity measurements for the WGS reaction were carried out in a Microreactivity Pro apparatus (ICP/CSIC, Spain) and using the experimental setup previously described in detail.[30] The reaction feed composition used was 4.2 vol % CO/29.3 vol % H_2O/66.5 vol % He, and the total volume flow rate was 83.5 N mL/min, resulting in a GHSV of about 40 000 h^{-1} ($L/L_{cat}/h$). The catalyst particle size was between 0.1 and 0.2 mm, and the amount of catalyst sample used for each catalyst composition was 0.2 g. The reactions were carried out at atmospheric pressure and at temperatures in the 473−603 K range over a prereduced catalyst in H_2/Ar flow at 523 K for 2 h. The effluent stream from the reactor was directed to a mass spectrometer (Omnistar, Balzer) for online measurements of H_2, CO, and CO_2 gases. The purity of all gases used in catalytic experiments (e.g., H_2, Ar, CO, and He, Linde Gas-Greece) was higher than 99.95%.

2.2.1. SSITKA−DRIFTS Studies. Steady-state isotopic transient kinetic analysis coupled with DRIFTS (SSITKA−DRIFTS) studies were performed using a Perkin-Elmer Spectrum GX-II FTIR spectrometer equipped with a high-temperature controllable DRIFTS cell (Harrick, Praying Mantis) to record spectra under reaction conditions in an in situ manner. Signal averaging was set to 50 scans per spectrum, and the spectra were collected in the 4000−500 cm^{-1} range at the rate of 0.2 scans/s (MCT detector) and a 2 cm^{-1} resolution. The background spectrum of the solid was taken under 29.3 vol % H_2O/Ar flow (200 mL/min) at the desired reaction temperature. The response time of the DRIFTS reactor cell (~40 mg Pt/CeO_2) under the present experimental conditions (200 mL/min, T = 473−573 K) was about 5 s. SSITKA−DRIFTS experiments to follow the carbon path of WGS were performed using the DRIFTS reactor cell and involved the switch 4.2 vol % ^{12}CO/29.3 vol % H_2O/1 vol % He/Ar (T, 30 min) → 4.2 vol % ^{13}CO/29.3 vol % H_2O/Ar (T, t) (use of ^{13}CO gas, 99.5 atom % ^{13}C, Spectra Gases). These studies allowed determining the chemical composition and structure of active reaction intermediates and that of inactive (spectator) species of the WGS reaction. For the same SSITKA experiment, the output of the DRIFTS cell could be connected to an

dx.doi.org/10.1021/jp201773a |J. Phys. Chem. C XXXX, XXX, 000–000

Table 1. Textural Properties and Metal Dispersion of Supported-Pt Catalysts

sample	d_c (nm)[a]	SSA, $m^2\ g^{-1}$	Pt dispersion D (%)	Pt mean particle size d_{Pt} (nm)[b]
0.5 wt % Pt/CeO_2	13.0	62.0	54.0	2.0
0.5 wt % Pt/CeO_2−TiO_2	20.0[c]	62.0	60.0	1.8
0.5 wt % Pt/TiO_2	23.0[d]	65.0[d]	57.0	1.9

[a] Volume average support crystallite size (see section 2.1). [b] Using the following formula: d_{Pt} (nm) = 1.1/D. [c] Related to titania crystallites. [d] Titania support was treated at 773 K for 4 h before impregnation with Pt solution (see section 2.1).

online mass spectrometer for operando studies. The temperature used was 473 or 573 K. The collected DRIFTS spectra were smoothed in order to remove high-frequency noise, if necessary, and further analyzed using the software Spectrum (PerkinElmer) for Windows. Deconvolution of the thus-derived DRIFTS spectra was performed according to reported guidelines.[22,31]

2.2.2. SSITKA−Mass Spectrometry Studies. The isotopes used in the SSITKA−MS experiments were ^{13}CO (99.5 atom % ^{13}C, Spectra Gases) and deuterium oxide (D_2O, 99.96 atom % D, Aldrich). SSITKA−MS experiments were performed using two HPLC pumps (GILSON 307) for the addition of H_2O and D_2O to the reactor feed stream in the apparatus described elsewhere.[30] The SSITKA−MS technique was used to follow the hydrogen path of reaction according to the gas switch 29.3 vol % H_2O/4.2 vol % CO/1 vol % Kr/Ar (T, 30 min) → 29.3 vol % D_2O/4.2 vol % CO/Ar (T, t), and the carbon path according to the gas switch 29.3 vol % H_2O/4.2 vol % ^{12}CO/1 vol % He/Ar (T, 30 min) → 29.3 vol % H_2O/4.2 vol % ^{13}CO/Ar (T, t). The dry gas from the exit of a condenser (Peltier Gas Cooler, model ECP 1000, M&C TechGroup) placed downstream of the reactor was directed to the mass spectrometer for online recording of the H_2, CO, and CO_2 normal and isotope-containing (D, ^{13}C) gaseous species. The concentration (μmol/g) of active H-containing intermediates was estimated based on the transient response curves of H_2, HD, and Kr, the flow rate at the reactor outlet (200 N mL/min), and the mass of the catalyst (W = 0.025 g diluted with 0.175 g of silica) according to the mass balance equations reported elsewhere.[21,22,31,32] The quantification of the active C-containing intermediates was made in a similar manner to that used for the H-containing intermediates.[22]

3. RESULTS AND DISCUSSION

3.1. Catalyst Characterization. Table 1 shows the textural properties, metal (Pt) dispersion, and mean metal particle size (d_{Pt}, nm) of supported platinum catalysts. As shown in Table 1, all catalysts exhibit similar specific surface areas, ca. 62−65 $m^2 \cdot g^{-1}$. The X-ray diffractogram of CeO_2−TiO_2-supported Pt obtained[33] showed reflections corresponding to the crystalline anatase phase with two additional weak diffraction peaks corresponding to a crystalline ceria phase (strong lines at 28.5 and 33.1°, JCPDS 34-394). Given the fact that the ceria loading of 6.6 wt % corresponds only to 45% of the theoretical surface monolayer coverage of TiO_2, it is apparent that calcination of 6.6 wt % CeO_2−TiO_2 support at 873 K (see section 2.1) caused partly the formation of a 3D ceria structure. The dispersion of platinum in the reduced catalysts, as determined by H_2 chemisorption, changed only slightly (Table 1), thus the corresponding mean Pt particle size (ca. 1.8−2.0 nm).

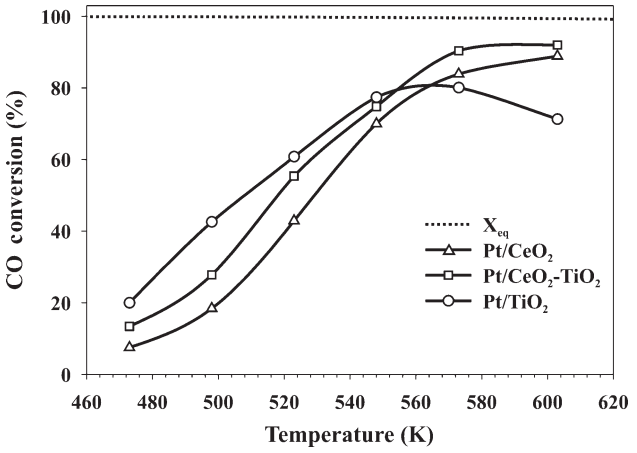

Figure 1. Effect of reaction temperature on the conversion of CO for the WGS reaction over Pt/CeO_2, Pt/CeO_2−TiO_2, and Pt/TiO_2 catalysts. The CO conversion (X_{eq}) versus T curve for equilibrium conditions (y_{CO}^{in} = 0.042 and y_{H2O}^{in} = 0.293) is also shown. Experimental conditions: W_{cat} = 0.2 g; feed composition 4.2 vol % CO, 29.3 vol % H_2O, He balance gas; total flow rate, Q = 83.5 N mL/min; GHSV ~ 40 000 h^{-1}.

3.2. Catalytic Activity Studies. The catalytic activity of the 0.5 wt % Pt/CeO_2, 0.5 wt % Pt/TiO_2, and 0.5 wt % Pt/CeO_2−TiO_2 catalysts for the water−gas shift reaction was evaluated in the 473−603 K range, and results in terms of CO conversion (X_{CO}, %) are shown in Figure 1. Significant differences in WGS activity are observed by varying the support chemical composition. The corresponding X_{CO} versus T profile for thermodynamic equilibrium at the present feed gas composition used is also given (X_{eq}, Figure 1). The thermodynamic equilibrium curve was derived using equilibrium constant (K_{eq}) values and appropriate mass balances as reported.[32] This curve shows that below 473 K full CO conversion can be achieved, whereas a minor decrease in the CO conversion by less than 1% unit is noticed at 603 K.

In the 473−548 K range, Pt/CeO_2 was found to be the least active catalyst, whereas Pt/TiO_2 was the most active (Figure 1). At temperatures above 548 K, while Pt/CeO_2 and Pt/CeO_2−TiO_2 approach equilibrium values, Pt/TiO_2 shows a reduced activity. The latter result is not due to any external or internal mass and heat transport resistance effects as evidenced by the use of the criteria reported in our recent work.[22] A similar behavior was also reported for the same catalysts after using the feed gas composition 28 vol % H_2/0.1 vol % CH_4/4.4 vol % CO/29.6 vol % H_2O/N_2.[33] It is speculated that the long-term exposure of Pt/TiO_2 at T > 548 K under the high level of water content present in the WGS reaction feed stream may cause modifications in the surface structure of titania, where, as will be shown later on, these would affect the reactivity and number density of active reaction sites of WGS formed in TiO_2 support. In addition, accumulation of adsorbed carbonate species (spectators) competing for the same catalytic sites as other active reaction intermediates does occur, as supported by the present in situ SSITKA−DRIFTS and SSITKA−MS studies to be reported in the following sections.

The higher CO conversion observed in Pt/TiO_2 compared to Pt/CeO_2 at T < 548 K, where both catalysts have similar mean Pt

dx.doi.org/10.1021/jp201773a |J. Phys. Chem. C XXXX, XXX, 000–000

particle sizes (Table 1), is an important result given the fact that Pt/CeO_2 is considered to be among the most effective catalysts for low-temperature WGS reaction.[8−10,34] It should be also noted that Pt supported on CeO_2-TiO_2 shows higher activity with respect to Pt/TiO_2 at $T > 548$ K. It was observed that Pt/CeO_2-TiO_2 catalyst showed the highest activity in terms of CO conversion and TOF (s^{-1}) when compared to Pt/CeO_2 and Pt/TiO_2 in the 490−575 K range after using a simulated reformate gas mixture.[33]

The specific kinetic reaction rate ($X_{CO} < 20\%$) obtained for the Pt/CeO_2-TiO_2 catalyst at 473 K was found to be 4.2×10^{-5} $mol \cdot s^{-1} \cdot g_{cat}^{-1}$, whereas that for the Pt/CeO_2 and Pt/TiO_2 was 2.3×10^{-5} and 6.2×10^{-5} $mol \cdot s^{-1} \cdot g_{cat}^{-1}$, respectively. The value of the specific kinetic reaction rate obtained using the mixing rule, $R_{Ce-Ti} = xR_{Ti} + (1 - x)R_{Ce}$, where x is the titania weight fraction in the TiO_2-CeO_2 support composition, and R_{Ce-Ti}, R_{Ti}, and R_{Ce} are the specific reaction rates of CO consumption ($mol \cdot s^{-1} \cdot g_{cat}^{-1}$) for CeO_2-TiO_2-, TiO_2-, and CeO_2-supported-Pt catalysts, respectively, was found to be 2.6×10^{-5} $mol \cdot s^{-1} \cdot g_{cat}^{-1}$. The latter value is only 62% of the experimental value estimated. This result indicates that Pt/CeO_2-TiO_2 does not behave as a physical mixture of Pt/CeO_2 and Pt/TiO_2 solids, but a positive synergy between the oxidic phases and the Pt metal surface exists. The intrinsic reasons of such synergy will be discussed in a subsequent section. A critical comparison of the obtained kinetic rates on the present Pt/CeO_2 and Pt/TiO_2 catalysts with corresponding ones reported in the literature is meaningful only when this is performed for the same feed gas composition and reaction temperature or with known reaction orders with respect to the reactants CO and H_2O and kinetic rate constant ($k = A \exp(-E_{app}/RT)$); thus, an extrapolation could be made. Panagiotopoulou and Kondarides[35] reported a kinetic rate at 493 K of 4.08×10^{-6} mol/g·s on a 0.5 wt % Pt/TiO_2 catalyst, whereas for the present catalyst at the same temperature, a kinetic rate of 9.0×10^{-6} mol/g·s was estimated. However, in the present study the H_2O feed concentration was about three times larger and the CO concentration was only 30% larger than the corresponding values used.[35] Considering the facts that the reaction order with respect to water was found to be unity,[21] the kinetic rate does not depend on the Pt particle size[36] but on the primary crystal of TiO_2,[37] and the present TiO_2 and that used (P25 Degussa)[35] have very similar primary crystal sizes (25 vs 23 nm (Table 1)), then it is estimated that the kinetic reaction rates obtained for the two catalysts are in very good agreement. Kinetic rates of WGS on various Pt/CeO_2 catalysts were reported in a review paper for various feed gas compositions (including H_2 and CO_2) and reaction temperatures.[38] It is interesting to compare the kinetic rates of the present 0.5 wt % Pt/CeO_2 catalyst at 523 K with a 0.5 wt % Pt/CeO_2[39] which had a very similar Pt dispersion (46%) as the present one (54%) but largely different ceria textural and structural properties (BET = 8 m^2/g, d_{CeO2} = 18.5 nm to be compared to 62.0 m^2/g and 13.0 nm, respectively). For the present catalyst, a kinetic reaction rate of 8.6×10^{-5} mol/g·s was obtained, whereas for the Pt/CeO_2[39] a value of 2.0×10^{-5} mol/g·s was obtained after correcting for the dependence of reaction rate on water feed concentration (reaction order of unity). It is very clear from this comparison the strong dependence of reaction rate of WGS on the structural properties of ceria support.

3.3. SSITKA−DRIFTS Studies. In order to determine the chemical composition of the active carbon-containing intermediates found in the WGS reaction mechanism, SSITKA−DRIFTS experiments were performed (see section 2.2.1). The IR bands corresponding to a given vibrational mode of an active species must show the red isotopic shift due to the replacement of ^{12}C-containing active intermediates with the corresponding ^{13}C-containing species during the switch $^{12}CO/H_2O \rightarrow {}^{13}CO/H_2O$. In the case that the particular species is not active, thus a spectator, the spectra under the isotope-labeled feed should not exhibit the red isotopic shift, and therefore the same spectrum as that observed under the $^{12}CO/H_2O$ treatment will be observed. However, an adsorbed spectator species formed on the catalyst surface which could interact *reversibly* with the isotope reactant species (e.g., ^{13}CO) would result in the observation of the red isotopic shift. Thus, other experiments should be performed to assign precisely the role of such an adsorbed species as being an active or spectator, as recently illustrated for the WGS reaction over supported-Pt catalysts.[22−24]

3.3.1. SSITKA−DRIFTS at 473 K. SSITKA−DRIFTS spectra recorded under the $^{12}CO/H_2O$ feed stream at 473 K for the three catalysts in the 2250−1850 cm^{-1} range, which corresponds to the C−O stretching vibrational mode of various types of Pt-bound carbon monoxide, are presented in Figure 2a−c. Deconvoluted spectra under both reaction feed compositions are also shown. All spectra recorded under the $^{12}CO/H_2O$ steady-state reaction conditions (30 min on stream) are presented by a solid line, while the deconvoluted ones corresponding to the $^{13}CO/H_2O$ treatment (30 min) are presented by a dashed line (bottom graph). The infrared bands centered at 2180 and 2120 cm^{-1}, labeled as 1 and 2, respectively, are due to the ^{12}CO gas phase.[40] For the Pt/CeO_2 catalyst (Figure 2a), the intense band centered at 2058 cm^{-1} (band 3) is related to a high-frequency (HF) linearly bound CO on Pt. The wide IR band (2040−1900 cm^{-1}) after deconvolution gives a small infrared band at 2030 cm^{-1} (band 4), which is assigned to a low-frequency (LF) linearly bound CO on Pt atoms present in small platinum particles (P_S) of low coordination ($d_{Pt} < 15$ Å),[41] and an infrared band 5 at 2000 cm^{-1}, which is attributed to CO adsorbed on Pt sites of low coordination in very small particles (P_{VS}).[41] Such Pt sites could be found at the periphery of a metal−support interface. In general, linear-CO adsorption does not lead to infrared bands in this spectral region. In fact, linear-CO adsorption gives bands in the 2100−2000 cm^{-1} range, whereas the ν(CO) region of bridging CO is located near 1850 cm^{-1}. Bazin et al.[41] proposed that infrared band 5 is due to adsorption of CO on isolated very low-coordinated Pt atoms in strong interaction with the support.

Similarly, the Pt/CeO_2-TiO_2 catalyst shows two IR bands centered at 2080 and 2033 cm^{-1} (Figure 2b, bands 3 and 4) related to linear adsorbed CO on Pt^0 and on small platinum particles (P_S), respectively. In the case of Pt/TiO_2 (Figure 2c), only the IR band corresponding to HF-linear adsorbed CO (band 3) centered at 2062 cm^{-1} is observed, accompanied by a shoulder below 2000 cm^{-1}, which is due to LF-linear adsorbed CO. As depicted in Figure 2a−c (bottom graphs), all IR bands described above show the red isotopic shift upon replacement of the ^{12}CO with ^{13}CO (SSITKA switch). Based only on the observed red isotopic shift, it cannot be safely said that these species are all active intermediates, as previously discussed. The reversible adsorption of CO on Pt implies that the isotopic shift observed could be due also to the following simple exchange reaction: $^{12}CO_{ads} + {}^{13}CO_{gas} \leftrightarrow {}^{13}CO_{ads} + {}^{12}CO_{gas}$. However, in agreement with our previous studies,[21,22,31] and what is mentioned in the literature,[42] one adsorbed CO species must at least be considered as an active intermediate of the C-path of the WGS reaction. This species reacts at the Pt−support interface according to a bifunctional mode catalytic process, where active sites

dx.doi.org/10.1021/jp201773a |J. Phys. Chem. C XXXX, XXX, 000–000

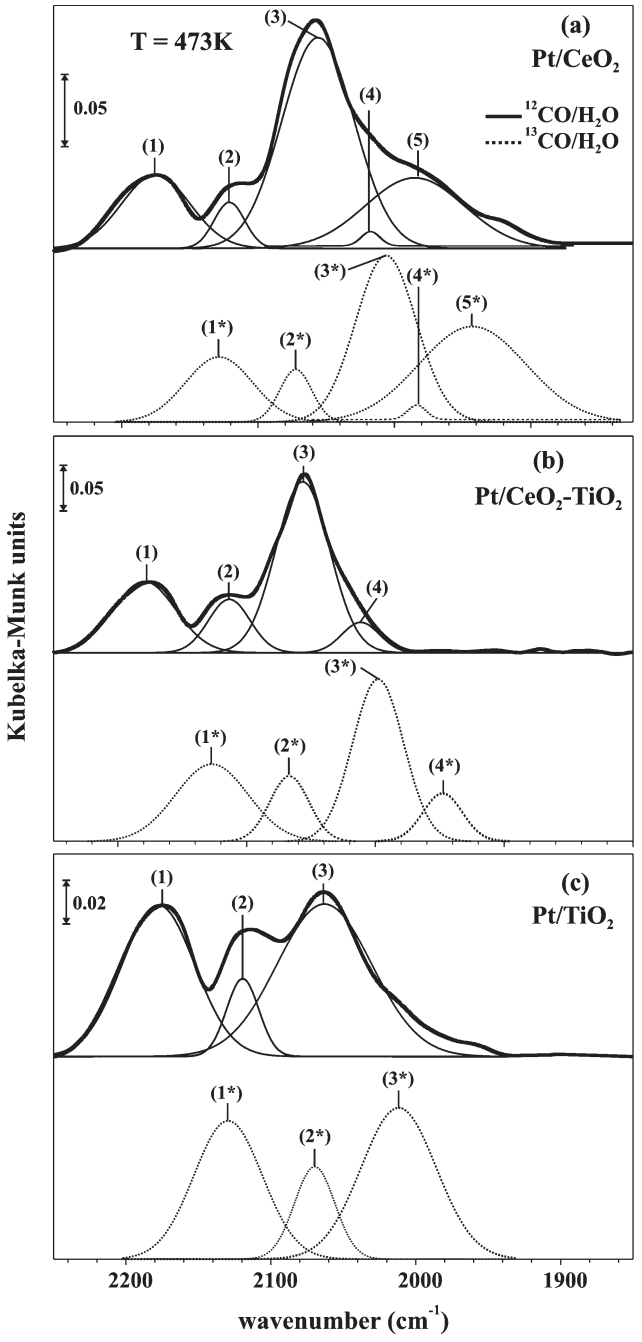

Figure 2. In situ DRIFTS spectra recorded in the 2250−1850 cm^{-1} range over (a) Pt/CeO_2, (b) Pt/CeO_2-TiO_2, and (c) Pt/TiO_2 catalysts under SSITKA WGS reaction conditions at 473 K. Solid-line spectra: 4.2 vol % ^{12}CO/29.3 vol % H_2O/Ar/He; dashed-line spectra: 4.2 vol % ^{13}CO/29.3 vol % H_2O/Ar. Deconvolution and curve fitting of recorded DRIFTS spectra are also provided (bottom graphs).

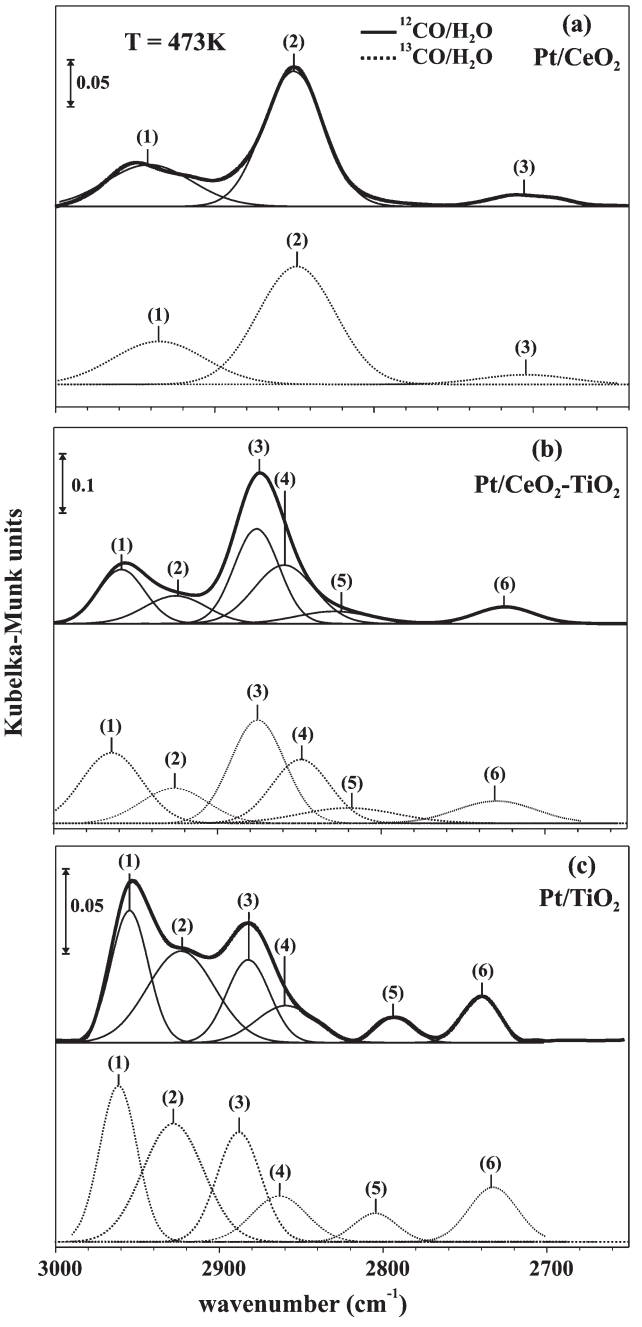

Figure 3. In situ DRIFTS spectra recorded in the 3000−2650 cm^{-1} range over (a) Pt/CeO_2, (b) Pt/CeO_2-TiO_2, and (c) Pt/TiO_2 catalysts under SSITKA WGS reaction conditions at 473 K. Solid-line spectra: 4.2 vol % ^{12}CO/29.3 vol % H_2O/Ar/He; dashed-line spectra: 4.2 vol % ^{13}CO/29.3 vol % H_2O/Ar. Deconvolution and curve fitting of recorded DRIFTS spectra are also provided (bottom graphs).

are present in both the metal and support. It is worth noting the different CO infrared bands obtained for each catalyst, indicating different interactions between Pt particles of similar size (see Table 1) and the CO species. These interactions depend on the support chemical composition. The Pt/CeO_2-TiO_2 catalyst shows the presence of a HF-linear CO at 2080 cm^{-1} (band 3), the highest frequency by 20 cm^{-1} compared to the other two catalysts (νCO of Pt/CeO_2 > νCO of Pt/TiO_2), indicating that the mixed oxide support is more electropositive than the bare oxides of ceria and titania.

Characteristic νCH stretching mode IR bands recorded in the 3000−2650 cm^{-1} range are due to adsorbed formate species (HCOO) formed under WGS reaction at 473 K (Figure 3a−c). Three infrared absorption bands are expected for a given type of formate adsorbed on a metal oxide. The most intense IR band appears around 2850 cm^{-1} and is related to the combination of δCH and νOCO_{as}, a band at 2950 cm^{-1} corresponds to the νCH

dx.doi.org/10.1021/jp201773a |J. Phys. Chem. C XXXX, XXX, 000–000

vibrational mode, and a weak IR band at 2720 cm^{-1} is due to the combination of $\delta CH + \nu OCO_s$. The assignment of the various vibrational modes of formate species was based on well-documented literature data.[15,40,42−49] As can be seen in Figure 3a, Pt/CeO_2 presents only one type of formate species showing the three characteristic infrared bands (2949, 2850, and 2710 cm^{-1}). On the contrary, six IR bands were recorded on Pt/CeO_2-TiO_2 and Pt/TiO_2 catalysts under the nonisotopic feed stream ($^{12}CO/H_2O$) as depicted in Figures 3b and 3c. These IR bands are assigned to two different kinds of formate species, e.g., bidentate and bridged formate, or to the same formate structure with a different local chemical environment.[50,51] Deconvolution and curve fitting of the spectra obtained under both the $^{12}CO/H_2O$ and $^{13}CO/H_2O$ reaction feed streams resulted in no measurable red isotopic shift in any of the IR bands for all three catalysts. Meunier et al.[52,53] based on SSITKA studies have reported that on a 2 wt % Pt/CeO_2 catalyst prepared by a homogeneous precipitation of Pt(II) in urea method, while at 433 K formate was practically an inactive species, as the present case at 473 K, formate was found to be an active reaction intermediate at 493 K. The authors stated that over quite a narrow temperature range, the kinetic importance of a surface species can be dramatically different, and therefore caution is required when attempting to generalize the reaction mechanism based on data using different reaction temperatures or feed compositions, or even differently prepared and pretreated (e.g., calcinations and reduction conditions) catalysts having the same nominal composition.

Figure 4a−c shows DRIFTS spectra for the three catalysts in the 1600−1200 cm^{-1} region associated with the stretching (symmetric and asymmetric) and rocking vibrational modes of the O−C−O group of adsorbed carbonate, formate, and carboxylate species (COOH) formed under WGS reaction at 473 K.[15,40,42−49] Due to the complexity regarding the clear assignment of IR bands in this region, an accurate deconvolution and curve fitting procedure was performed in order to resolve and differentiate the various adsorbed species. Six IR bands can be seen in all three supported-Pt catalysts investigated. Band 1 is related to the νOCO_{as} vibrational mode of formate, bands 2, 3, and 4 are related to νOCO_s of different carbonate species, and bands 5 and 6 are related to δCH and νOCO_s vibrational modes of formate species.[15,40,42−49] Vibrational frequencies due to formates and carbonates appear to depend on the chemical composition of support. In the case of Pt/CeO_2 (Figure 4a), the most intense IR bands observed at 1593 (band 1), 1380 (band 5), and 1333 cm^{-1} (band 6) are assigned to formates, whereas bands at 1570 (band 2), 1522 (band 3), and 1485 cm^{-1} (band 4) are assigned to carbonate species. In the case of Pt/TiO_2 (Figure 4c), IR bands related to formates are now located at 1570, 1390, and 1358 cm^{-1}, while those corresponding to carbonates are at 1529, 1478, and 1441 cm^{-1}. In the case of Pt/CeO_2-TiO_2, similar IR bands to those obtained with Pt supported on CeO_2 and TiO_2 alone are observed (Figure 4b).

After the new steady-state under the isotopic $^{13}CO/H_2O$ gas mixture was reached (Figure 4a−c, bottom graph, dashed-line spectra), it is seen that only two IR bands (labeled as 2* and 4*) related to carbonate species showed the red isotopic shift. This result is related to CO_2 readsorption effects, where only part of carbonate species formed under WGS reaction conditions is reversibly chemisorbed, as will be further demonstrated and discussed. The irreversibly chemisorbed carbonates could explain the drop in activity for Pt/TiO_2 at reaction temperatures higher than 548 K, as opposed to the other two catalyst formulations (Figure 1).

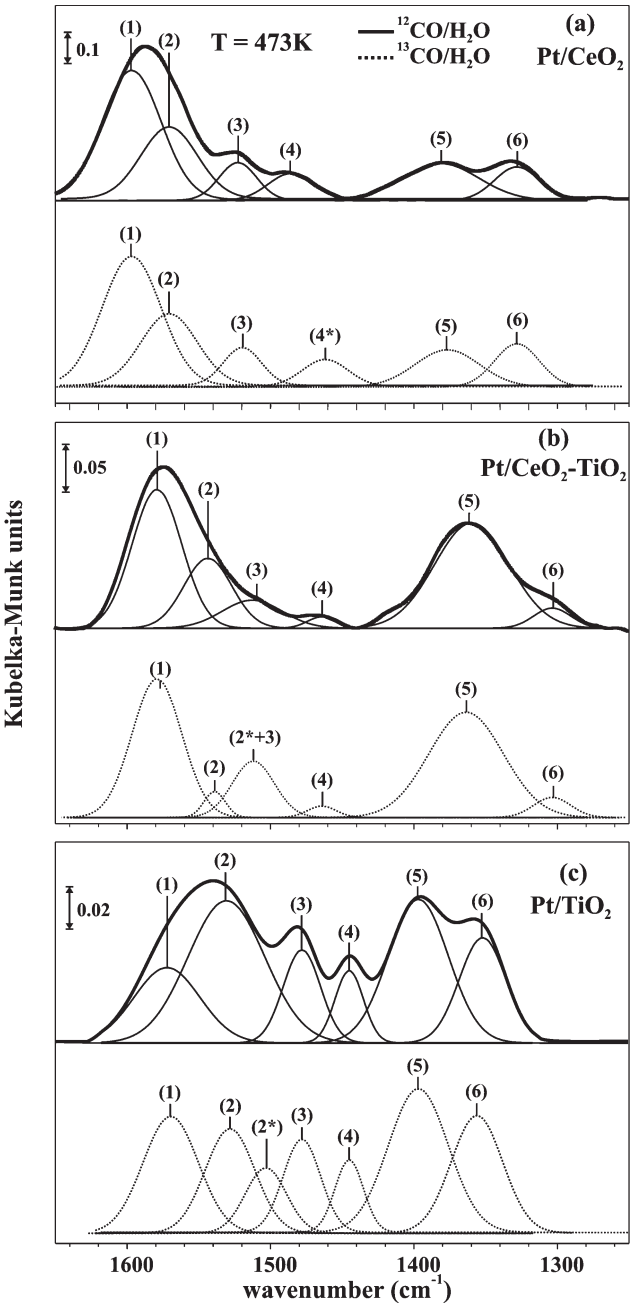

Figure 4. In situ DRIFTS spectra recorded in the 1650−1250 cm^{-1} range over (a) Pt/CeO_2, (b) Pt/CeO_2-TiO_2, and (c) Pt/TiO_2 catalysts under SSITKA WGS reaction conditions at 473 K. Solid-line spectra: 4.2 vol % ^{12}CO/29.3 vol % H_2O/Ar/He; dashed-line spectra: 4.2 vol % ^{13}CO/29.3 vol % H_2O/Ar. Deconvolution and curve fitting of recorded DRIFTS spectra are also provided (bottom graphs).

3.3.2. SSITKA−DRIFTS at 573 K. Figure 5a−c shows IR bands in the 2250−1800 cm^{-1} range corresponding to CO adsorbed on platinum particles. In the case of Pt/CeO_2, the most intense IR band recorded at 2060 cm^{-1} under $^{12}CO/H_2O$ reaction conditions (band 3, Figure 5a) corresponds to a HF-linear adsorbed CO on Pt^o. Infrared band 5, which is related to adsorbed CO on P_{VS} particles, shows a decreased integral absorbance compared to that observed at 473 K. On the contrary, IR band 4 (2023 cm^{-1})

dx.doi.org/10.1021/jp201773a |J. Phys. Chem. C XXXX, XXX, 000–000

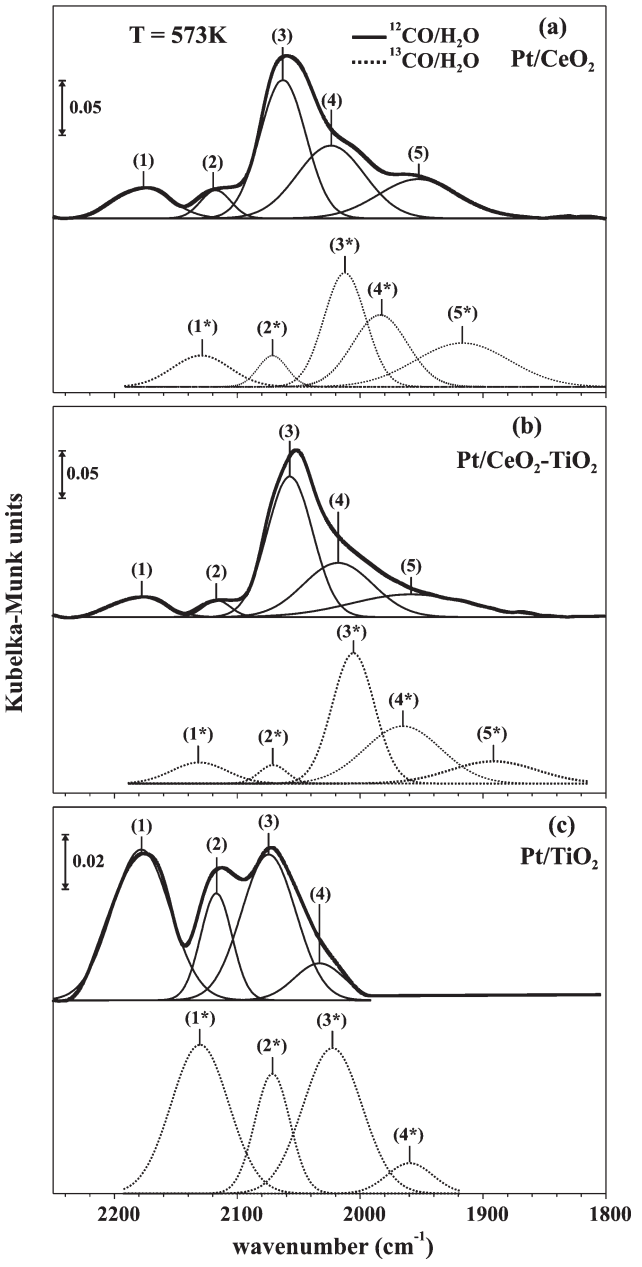

Figure 5. In situ DRIFTS spectra recorded in the 2250−1800 cm^{-1} range over (a) Pt/CeO_2, (b) Pt/CeO_2-TiO_2, and (c) Pt/TiO_2 catalysts under SSITKA WGS reaction conditions at 573 K. Solid-line spectra: 4.2 vol % ^{12}CO/29.3 vol % H_2O/Ar/He; dashed-line spectra: 4.2 vol % ^{13}CO/29.3 vol % H_2O/Ar. Deconvolution and curve fitting of recorded DRIFTS spectra are also provided (bottom graphs).

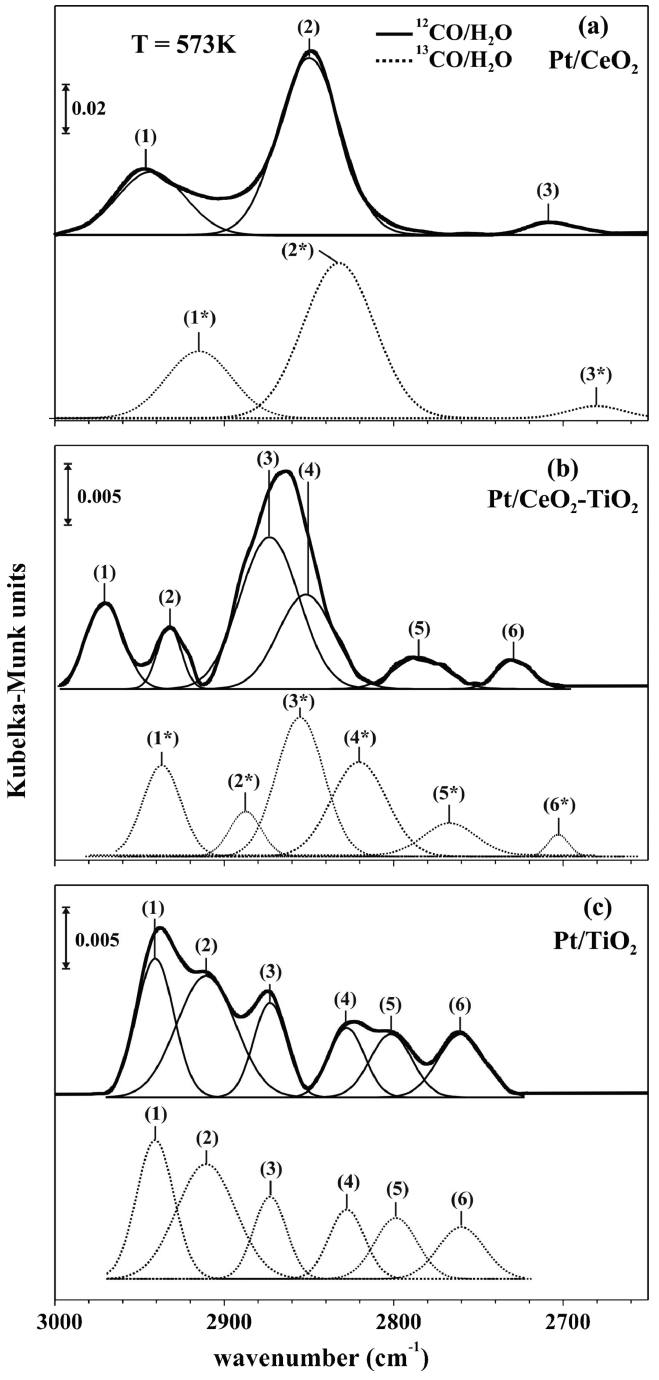

Figure 6. In situ DRIFTS spectra recorded in the 3000−2650 cm^{-1} range over (a) Pt/CeO_2, (b) Pt/CeO_2-TiO_2, and (c) Pt/TiO_2 catalysts under SSITKA WGS reaction conditions at 573 K. Solid-line spectra: 4.2 vol % ^{12}CO/29.3 vol % H_2O/Ar/He; dashed-line spectra: 4.2 vol % ^{13}CO/29.3 vol % H_2O/Ar. Deconvolution and curve fitting of recorded DRIFTS spectra are also provided (bottom graphs).

related to adsorbed CO on P_S particles presents a significantly increased integral absorbance (compare Figures 2a and 5a).

In the case of Pt/TiO_2, the IR spectrum recorded under $^{12}CO/H_2O$ (Figure 5c) shows an infrared band at 2039 cm^{-1} (band 4) attributed to a LF-linear adsorbed CO on step sites of Pt. This band appeared as a shoulder of band 3 at 473 K (Figure 2c). It is noted the red shift observed in the IR band associated with the HF-linear adsorbed CO obtained on Pt/CeO_2-TiO_2 and Pt/TiO_2 catalysts at 573 and 473 K; 2055 and 2062 cm^{-1} compared to 2063 and 2079 cm^{-1}, respectively. This could be attributed to a surface coverage effect via an increase in the dipole−dipole coupling between adsorbed CO species at neighboring sites.[54,55] The Pt/CeO_2-TiO_2 catalyst shows IR bands (Figure 5b) corresponding to the same kinds of adsorbed CO as those observed in Pt/CeO_2 (Figure 5a) and Pt/TiO_2 (Figure 5c) solids but with different ratios in their surface concentration under WGS reaction conditions. As observed at 473 K (Figure 2a−c), all IR bands related to adsorbed CO showed also the red isotopic shift at 573 K (Figure 5a−c).

dx.doi.org/10.1021/jp201773a |J. Phys. Chem. C XXXX, XXX, 000–000

Three characteristic IR bands due to $\delta CH + \nu OCO_{as}$, νCH, and $\delta CH + \nu OCO_s$ vibrational modes and which are related to one kind of formate formed on the CeO_2 support were observed on Pt/CeO_2 (Figure 6a) as in the case of reaction performed at 473 K (Figure 3a). Deconvolution and curve fitting of the spectra recorded at 573 K for Pt/CeO_2−TiO_2 (Figure 6b) resulted in six IR bands assigned to two different kinds of adsorbed formate species as in the case of WGS at 473 K (Figure 3b). Deconvolution of the spectra recorded under the $^{13}CO/H_2O$ treatment of the Pt/CeO_2 and Pt/CeO_2−TiO_2 catalysts (Figure 6a, b, dashed-line) clearly shows the isotopic red shift for all bands recorded, a result opposite to that seen at 473 K. On the contrary, the six IR bands recorded on Pt/TiO_2 (Figure 6c) do not show any isotopic red shift under the $^{13}CO/H_2O$ treatment of the catalyst as similarly observed in the case of WGS performed at 473 K. As will be discussed also in section 3.5, formate species on Pt/TiO_2 appear to be merely spectator species at both low-T (473 K) and high-T (573 K) of the WGS reaction. On the other hand, formate species appear to switch from being active intermediates at 573 K to inactive species at 473 K over the Pt/CeO_2 and Pt/CeO_2−TiO_2 catalysts.

Similar IR bands to those obtained at 473 K (Figure 4a−c) were recorded at the high-T of 573 K in the 1650−1250 cm^{-1} range (Figure 7a−c). Infrared bands 1, 4, 5, and 6 are assigned to the vibrational modes of formates, whereas bands 2 and 3 to carbonate species. The IR spectra recorded on Pt/CeO_2 and Pt/CeO_2−TiO_2 (Figure 7a, b) under the $^{13}CO/H_2O$ gas mixture showed the red isotopic shift. On the other hand, Pt/TiO_2 shows a similar behavior to that obtained at 473 K (Figure 4c) having only the IR bands related to a carbonate species to exhibit the red isotopic shift (band 2*, Figure 7c). Also, it is important to note that a second kind of carbonate species formed does not provide the red isotopic shift (band 3), clearly indicating that this carbonate should be considered as an inactive species.

Based on the SSITKA−DRIFTS studies reported at 473 K (Figures 2−4) and 573 K (Figures 5−7), it is apparent that depending on reaction temperature and catalyst support composition, the chemical composition of the active species found in the carbon path of the WGS reaction is different. As mentioned previously, the red isotopic shift by itself cannot be considered as a safe criterion to assign whether the related adsorbed species can be considered as active reaction intermediates. Thus, even though carbonates (IR bands 2 and 3, Figures 4, 7) had given the red isotopic shift at both reaction temperatures, these species may not be true active reaction intermediates as will be discussed below.

3.4. SSITKA−Mass Spectrometry Studies. The SSITKA−MS experiments were used to follow the hydrogen path and carbon path of the WGS reaction mechanism from the reactants (H_2O and CO) to the gas products (H_2 and CO_2) under kinetic regime conditions (CO conversion <15%), following, respectively, the gas switch $H_2O/CO/Ar/Kr$ (T, 30 min) → $D_2O/CO/Ar$ (T, t) and $H_2O/^{12}CO/Ar/He$ (T, 30 min) → $H_2O/^{13}CO/Ar$ (T, t) at the temperatures of 473 and 573 K.

3.4.1. Carbon Path of the WGS Reaction. Figure 8a−c shows normalized dynamic response curves, Z, of ^{12}CO, ^{13}CO, $^{12}CO_2$, $^{13}CO_2$, and He recorded upon the isotopic switch over the Pt/TiO_2 (Figure 8a), Pt/CeO_2−TiO_2 (Figure 8b), and Pt/CeO_2 (Figure 8c) catalysts at 473 K. A relatively rapid decay of the $^{12}CO_2$ signal accompanied by an increase in $^{13}CO_2$ was observed. Both curves cross each other at $Z = 0.5$ as predicted by the SSITKA theory.[21,22,56] The concentration of C-containing active intermediates ($\mu mol/g_{cat}$) is estimated via a material balance equation,[22,31,32] which is proved to be proportional to the area difference between the $^{12}CO_2$ and He transient response curves. This concentration is related to all C-containing intermediates formed during WGS and leading to the CO_2(g) formation, such as adsorbed CO, carbonate, and/or formate. It is important to note that the $^{12}CO_2$(g) and $^{13}CO_2$(g) response curves are influenced by the kinetics of adsorption/desorption of CO_2 on active and nonactive catalytic sites,[56] and this will be discussed in the following section 3.4.2. Table 2 summarizes

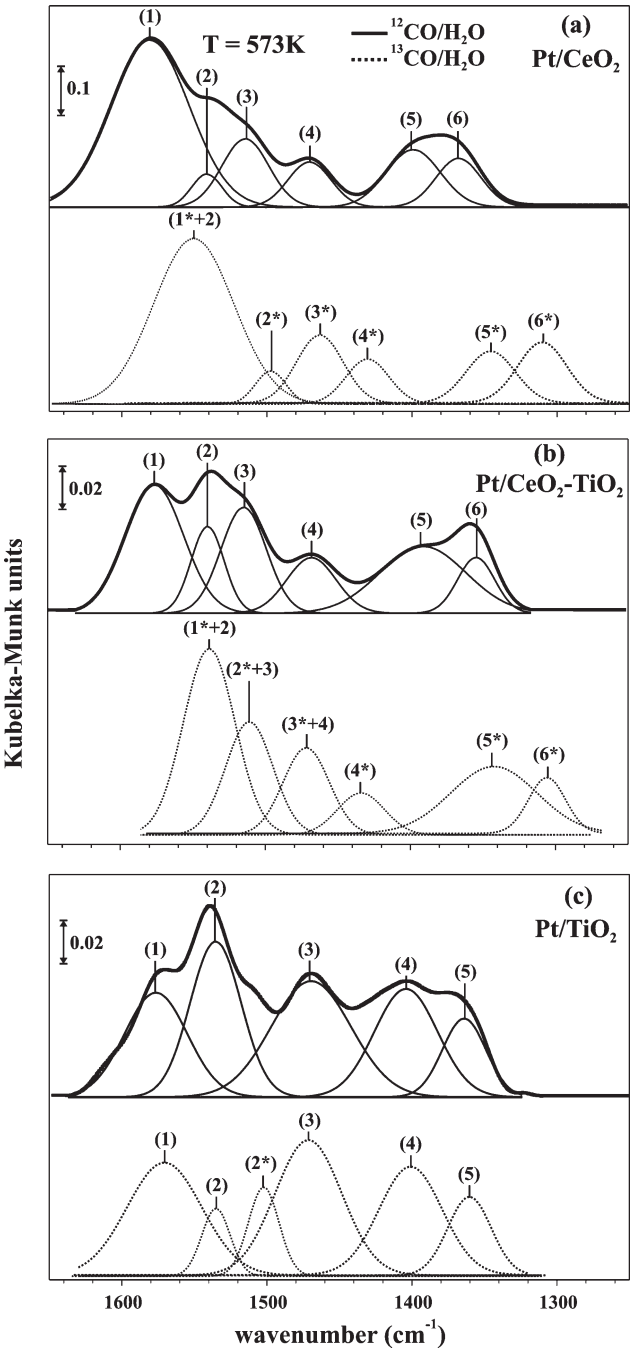

Figure 7. In situ DRIFTS spectra recorded in the 1650−1250 cm^{-1} range over (a) Pt/CeO_2, (b) Pt/CeO_2−TiO_2, and (c) Pt/TiO_2 catalysts under SSITKA WGS reaction conditions at 573 K. Solid-line spectra: 4.2 vol % ^{12}CO/29.3 vol % H_2O/Ar/He; dashed-line spectra: 4.2 vol % ^{13}CO/29.3 vol % H_2O/Ar. Deconvolution and curve fitting of recorded DRIFTS spectra are also provided (bottom graphs).

dx.doi.org/10.1021/jp201773a |J. Phys. Chem. C XXXX, XXX, 000–000

the concentration of active C-containing intermediates in terms of μmol/g_{cat} or surface coverage, θ, the latter based on the exposed surface area of Pt reported in Table 1 (D, %) for all three supported-Pt catalysts, after correcting for CO_2 readsorption effects (see section 3.4.2). The mean residence time of the active carbon-containing species, $\tau_{C\text{-pool}}$ (s) is also provided in Table 3, and it was estimated from the $Z(t)$ versus time transient response curves of CO_2 and He (Figure 8)[56] after correcting for CO_2 readsorption effects.

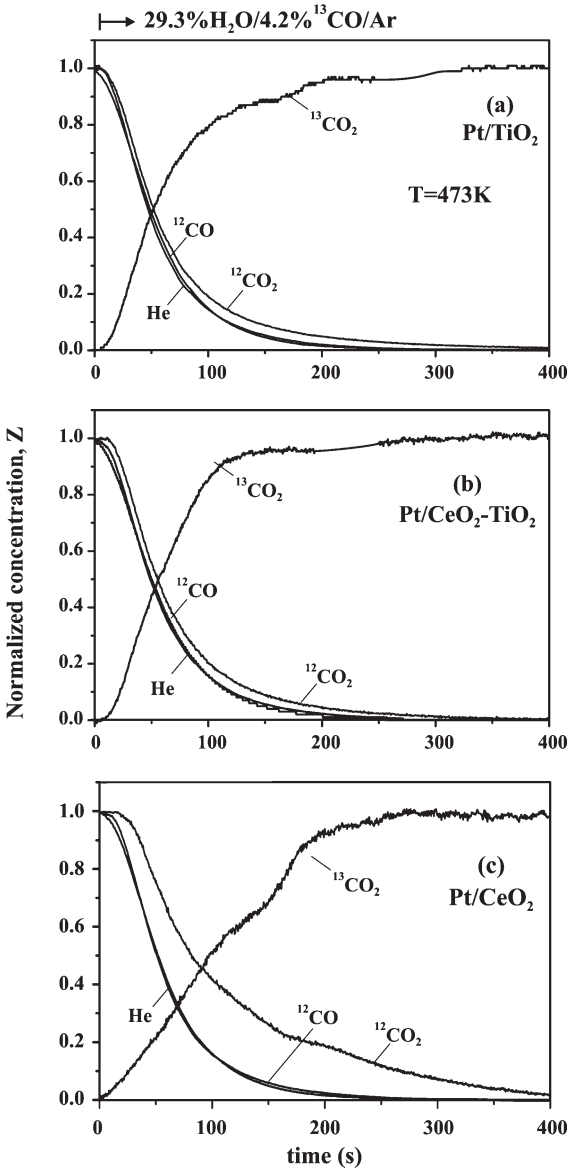

Figure 8. SSITKA-mass spectrometry experiments performed to estimate the concentration of active carbon-containing (C-pool) reaction intermediates found in the carbon path of the WGS reaction on (a) Pt/TiO_2, (b) Pt/CeO_2−TiO_2, and (c) Pt/CeO_2 catalysts at 473 K. Gas delivery sequence: 4.2 vol % ^{12}CO/29.3 vol % H_2O/Ar/He (30 min) → 4.2 vol % ^{13}CO/29.3 vol % H_2O/Ar (t).

As seen in Table 2, values of C-pool in terms of θ_C are in the 0.3−7.2 range for all three catalysts at 473 and 573 K. For the high-T of 573 K, it is clear that a large part of the active C-containing intermediates are formed along the platinum-support interface and/or on sites present within an active zone around the Pt nanoparticles. It is important to note that the concentration of these species at 573 K on Pt/TiO_2 is larger by a factor of 2.4 and 1.6, respectively, compared to Pt/CeO_2−TiO_2 and Pt/CeO_2 catalysts, a result that is consistent with the activity order observed at 573 K (Figure 1) at high CO conversions. The latter is true since a large concentration of an active reaction intermediate suggests that the site reactivity (k, rate constant) associated with this species is low, and vice versa. This reasoning, however, should consider also the dependence of the reaction kinetic rate on the concentration of other important reaction intermediates of WGS, such as the H-containing, a subject to be discussed in section 3.4.3.

The concentration (μmol/g_{cat}) of the reversibly adsorbed $^{12}CO_{ads}$ that is formed under WGS reaction conditions and is exchanged with gaseous $^{13}CO_g$ according to the following elementary reaction step 1

$$^{12}CO_{ads} + {}^{13}CO_g \leftrightarrow {}^{13}CO_{ads} + {}^{12}CO_g \qquad (1)$$

can be determined by applying the following material balance equation

$$N_{CO} = \left[F_T.\frac{y_{CO}{}^{f}(1 - X_{CO})}{W}\right]\int_0^{t^f} [Z_{CO}(t) - Z_{He}(t)]\, dt \ (\mathrm{mol/g_{cat}}) \qquad (2)$$

where F_T is the total molar flow rate of the reaction mixture at the exit of the reactor, $y_{CO}{}^{f}$ is the mole fraction of ^{12}CO in the

Table 3. Mean Residence Time, $\tau_{C\text{-ppol}}$ (s), of the Active Carbon-Containing (C-Pool) and $\tau_{H\text{-ppol}}$ (s) of Hydrogen-Containing (H-Pool) Intermediates of the WGS Reaction at 473 and 573 K (4.2 vol % CO/29.3 vol % H_2O/He) over the 0.5 wt % Pt/CeO_2, 0.5 wt % Pt/TiO_2, and 0.5 wt % Pt/CeO_2−TiO_2 Catalysts

	$\tau_{C\text{-pool}}$ (s)		$\tau_{H\text{-pool}}$ (s)	
catalyst	473 K	573 K	473 K	573 K
Pt/CeO_2	10.5	3.5	66.8	64.7
Pt/TiO_2	1.4	3.1	64.4	68.8
Pt/CeO_2−TiO_2	1.5	2.5	65.6	85.4

Table 2. Concentration of Active H-Containing, C-Containing,[a] and CO Precursor Reaction Intermediates Formed under Steady-State WGS Reaction (4.2 vol % CO/29.3 vol % H_2O/He; 473 or 573 K) on Supported-Pt Catalysts

	C-containing (μmol/g_{cat}) or (θ_C)[b]		CO precursor, N_{CO} (μmol/g_{cat}) or (θ_{CO})[b]		H-containing (μmol H/g_{cat}) or (θ_H)[b]	
catalyst	473 K	573 K	473 K	573 K	473 K	573 K
Pt/CeO_2	12.9 (0.9)	61.7 (4.5)	5 (0.4)	75 (7.4)	77 (5.6)	2816 (204)
Pt/TiO_2	4.6 (0.4)	93.9 (7.2)	3 (0.3)	99 (7.6)	77 (5.9)	2250 (172)
Pt/CeO_2−TiO_2	3.2 (0.28)	39.0 (3.0)	6 (0.5)	46 (3.7)	57 (4.3)	2766 (225)

[a] Corrected values from CO_2 readsorption effects (see Figure 9 and section 3.4.2). [b] In terms of surface monolayers of platinum.

dx.doi.org/10.1021/jp201773a |J. Phys. Chem. C XXXX, XXX, 000–000

$^{12}CO/H_2O$ feed stream, X_{CO} is the CO conversion, W is the mass (g) of catalyst used in the experiment, and $Z_{CO}(t)$ is a normalized concentration of ^{12}CO given by the following relationship

$$Z_{CO}(t) = \frac{y_{CO}(t)}{y_{CO}^{s.s.}} \quad (3)$$

which is estimated based on the recorded signal of $y_{CO}(t)$ under the $^{13}CO/H_2O$ gas mixture and the steady-state CO concentration, $y_{CO}^{s.s.}$, obtained at the reactor outlet. Table 2 reports the quantity N_{CO} termed "CO precursor" intermediates in terms of $\mu mol/g_{cat}$ or θ_{CO}. Since part of the adsorbed CO should be considered as active precursor intermediate that leads to the WGS reaction products, as will be discussed later, part of N_{CO} reflects the active adsorbed CO which provides the red isotopic shift in the SSITKA−DRIFTS experiment. Based on the results of the latter experiment (Figures 2 and 5), the red isotopic shift provided by the adsorbed CO was indeed observed. However, it is not possible to discriminate from these results which kinds of adsorbed CO must be considered as true active intermediates or spectator species, and which follow the elementary reaction step 1. It is seen that $\theta_{CO} = 0.3-0.5$ at the low-T of 473 K, whereas it is significantly larger than 1 ($\theta_{CO} = 3.7-7.6$) at the high-T of 573 K. At the latter reaction temperature values of θ_{CO} larger than unity for N_{CO} strongly indicate that besides the adsorbed CO on Pt there must be another adsorbed species formed on the support under WGS reaction conditions and which is able to interact reversibly with $^{13}CO(g)$. It was reported[9,21,31,32,42,45,57] that adsorbed CO can react reversibly with −OH groups of the support to form formate species, and it can also react directly with support surface lattice oxygen to form carbonate species, the latter decomposing into gaseous CO_2 according to the following elementary reaction steps:

$$CO_{ads} + OH\text{-}s \leftrightarrow HCOO\text{-}s \quad (4)$$

$$CO_{ads} + 2O^{-}\text{-}s \leftrightarrow [CO_3]^{2-}\text{-}s \quad (5)$$

$$[CO_3]^{2-}\text{-}s \leftrightarrow CO_2(g) + O^{-}\text{-}s + (\square/e^{-}) \quad (6)$$

$$CO_2(g) + O^{2-}\text{-}s \leftrightarrow [CO_3]^{2-}\text{-}s \quad (7)$$

where $(\square/e^{-})$ is an oxygen vacant site and s is a surface support catalytic site. In the case of Pt/TiO_2, only carbonate species provided the red isotopic shift (Figures 4c, 7c), strongly suggesting that reactions 5−7 can take place. On the contrary, at the high-T of 573 K, both Pt/CeO_2 and Pt/CeO_2-TiO_2 catalysts must be considered to promote reactions 4−7 in agreement with the SSITKA−DRIFTS studies which showed that formates and carbonates provided the red isotopic shift (Figures 6 and 7). According to reactions 5 and 6, carbonate contributes to the reduction of support. In addition, reaction step 6 is favored by the presence of Pt which participates in a charge transfer between Pt and O atoms of support at the Pt−support interface, thus reducing the bonding strength of Ce−O−Ce.[15] In other words, reaction step 6 is largely facilitated at the Pt−ceria interface, and it may not occur if carbonates are formed on sites far distant from the Pt−ceria interface. It is therefore suggested that at 473 K the N_{CO} quantity ($\theta_{CO} = 0.3-0.5$) obtained for all three supported Pt catalysts is due to an active adsorbed CO precursor species leading to CO_2 and H_2 via the "redox" and "associative formate" routes as will be discussed in section 3.5.

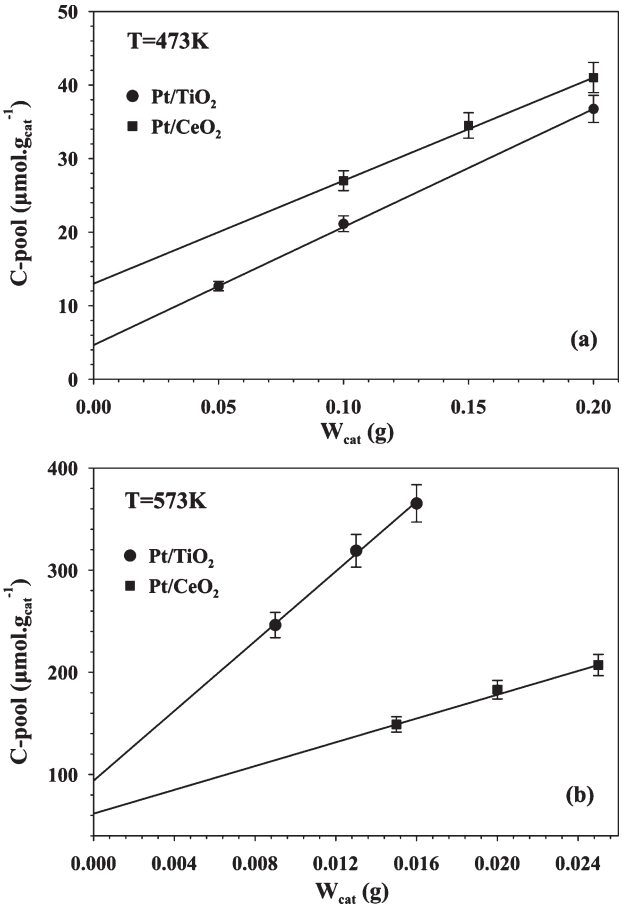

Figure 9. Dependence of the concentration ($\mu mol \cdot g_{cat}^{-1}$) of active carbon-containing (C-pool) reaction intermediates found in the carbon path of the WGS reaction on Pt/TiO_2 and Pt/CeO_2 catalysts on the amount of catalyst sample used in the SSITKA−MS experiments at T = 473 K (a) and T = 573 K (b). Extrapolation of the straight line to $W_{cat} = 0$ provides the concentration of active C-pool free of CO_2 readsorption effects.

3.4.2. CO_2 Readsorption Effects. To check the reversibility of CO_2 chemisorption step 6 on Pt/CeO_2 at 473 and 573 K, and to explain correctly the red isotopic shift due to carbonate species, the following experiments have been designed and performed:

(a) SSITKA−MS experiments similar to that presented in Figure 8 but using different amounts of catalyst (8−25 mg) diluted in SiO_2 so as to keep the same GHSV as that used in the experiment of Figure 8. Linear extrapolation of the concentration ($\mu mol/g_{cat}$) of C-containing intermediates to W_{cat} = 0.0 leads to the true concentration of C-containing intermediates in the absence of CO_2 readsorption on nonactive catalytic sites, thus avoiding overestimation of the C-pool.[56] Results for the Pt/CeO_2 and Pt/TiO_2 catalysts are presented in Figure 9 and reported in Table 2 for all three catalysts investigated. It is seen that readsorption of CO_2 does occur to a great extent in all catalysts, but to a larger degree on Pt/CeO_2 than Pt/TiO_2.

(b) Chemisorption of CO_2 at 473 and 573 K followed by isothermal desorption in He flow: x vol % CO_2/Ar/He (T, 30 min) → He (T, t). In this experiment, the CO_2 feed concentration used, x = 0.5 or 1.0 vol %, was that observed

dx.doi.org/10.1021/jp201773a | J. Phys. Chem. C XXXX, XXX, 000–000

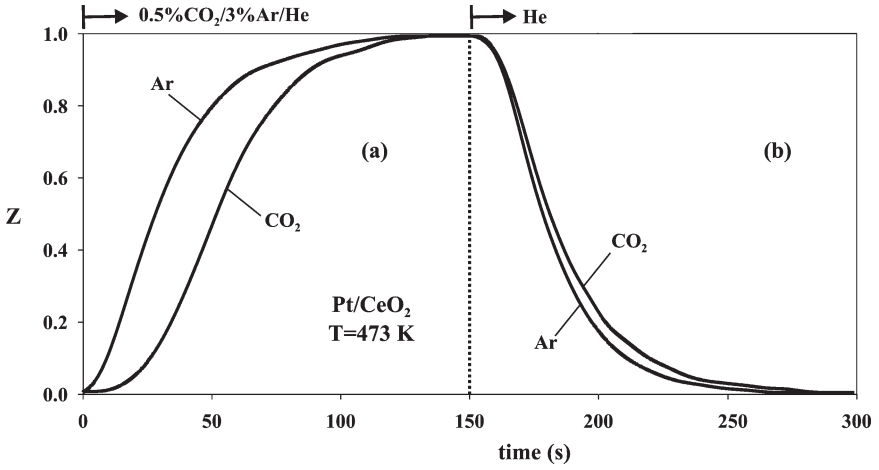

Figure 10. Transient isothermal (T = 473 K) dimensionless concentration (Z) response curves of CO_2 and Ar (tracer) during adsorption (a) and desorption (b) of carbon dioxide on a 0.5 wt % Pt/CeO_2 catalyst. Gas delivery sequence: He → 0.5 vol % CO_2/3 vol % Ar/He (473 K, 10 min) → He (473 K, t).

under steady-state WGS for the SSITKA−MS experiment (Figure 8) at 473 and 573 K, respectively.

Figure 10 presents the isothermal adsorption (Figure 10a) and desorption (Figure 10b) curves of CO_2 and that of tracer Ar gas obtained at 473 K on Pt/CeO_2 according to the experiment (b) described above. It is clearly seen that carbonate species formed upon CO_2 chemisorption at 473 K decompose according to reaction step 6 in He flow at the same temperature. However, it was found that only 25% of adsorbed CO_2 (Figure 10a, 40 μmol/g_{cat}) decomposes at 473 to CO_2(g) (Figure 10b), while the extent of desorption at 573 K was found to be significantly larger, 85%. These results are in harmony with the SSITKA−DRIFTS experiments (Figures 4a and 7a), where only part of the formed carbonate IR band gave the red isotopic shift. As will be shown in the following section 3.5, the redox mechanism involves the formation of a carbonate-type intermediate, which leads to CO_2(g) and an oxygen vacant site. This intermediate must be considered as the most populated active reaction intermediate of the carbon path of the WGS reaction according to the results reported in Table 2. Reversible chemisorption of CO_2(g) on the oxygen vacant sites cannot be excluded.[58]

3.4.3. Hydrogen Path of the WGS Reaction. Figure 11a−c presents transient concentration response curves of H_2, HD, D_2, and Kr obtained after the $^{12}CO/D_2O/Ar$ isotopic switch was made at 573 K over each of the three supported-Pt catalysts investigated. In all cases a large HD(g) signal was recorded, and the H_2(g) response curve lies well above that of Kr tracer gas. The appearance of HD(g) might be the result of (a) the recombination of adsorbed H and D on the Pt surface and (b) the exchange of H of −OH group of support with D from D_2(g) and/or D_2O(g) under the $^{12}CO/D_2O/Ar$ gas switch. These side exchange reactions which would overestimate the size of the H-pool were carefully checked experimentally as follows:

(a) A 30 vol% H_2O/Ar mixture was passed over each of the present supported-Pt catalysts (W = 0.025 g diluted with 0.175 g of silica) for 30 min, followed by a switch to the equivalent 30 vol % D_2O/Ar isotopic gas mixture at 573 K.

(b) The supported-Pt catalyst was first treated with 30% H_2O/Ar at 573 K for 30 min, followed by Ar purge for 10 min and then by 0.8 vol % D_2/Ar treatment at 573 K.

During the 30 vol % D_2O/Ar switch according to experiment (a) described above, no production of any HD or H_2 gas was observed. Figure 12 presents results of the HD(g) and H_2(g) response curves recorded under the Ar → 0.8 vol % D_2/Ar (t) gas switch at 573 K according to experiment (b) described above. It is clearly seen that a similar HD response in shape and position as that obtained under SSITKA (Figure 11) was observed. However, after integration of the HD and H_2 responses an amount of 5.8 μmol H/g_{cat} is obtained, which is much smaller than the value of 2816 μmol H/g_{cat} estimated for the active H-pool reported in Table 2. Therefore, it is more than clear that the large size of H-pool estimated at 473 and 573 K (Table 2) represents the active H-containing species that participate in the H-path of the WGS reaction and must be related to the support surface. It should be noted that any formation of HD(g) by exchange of H_2/D_2 on Pt during the 350 s of the transient (Figure 11) will not affect the correct measurement of H-containing intermediates using the H_2 and HD response curves, simply because reduction in the H_2 signal due to this exchange process would result in an equivalent increase in the HD signal.

It is seen from Table 2 that for the low-T of 473 K the surface coverage of active H-pool is in the range of $4.3 < \theta_H < 5.9$, and for Pt/CeO_2 formate (H-containing species) cannot be considered as an active intermediate (see section 3.4.1). Therefore, the active H-pool must largely reside on the ceria support, and the chemical nature of these species is −OH/H (from water dissociation) according to the redox mechanism to be presented in section 3.5. We have previously reported[31] that a "reactive zone" around the Pt nanoparticles must exist which contains the OH/H active species, where surface diffusion toward Pt must occur in order to form the dihydrogen gas product of the WGS reaction. In fact, by determining the total specific perimeter (cm/g) of supported-Pt particles (assuming hemispherical shape) as previously reported,[22] and considering a distance of about 2 Å between two adjacent −OH groups, the concentration of −OH groups present along the periphery of metal−support interface is estimated to be 3.2, 3.5, and 3.2 μmol·g_{cat}^{-1} for Pt/CeO_2, Pt/CeO_2-TiO_2, and Pt/TiO_2, respectively. These values are smaller than the ones reported for the size of the active H-pool (Table 2), clearly showing that there is a reactive zone

dx.doi.org/10.1021/jp201773a |J. Phys. Chem. C XXXX, XXX, 000–000

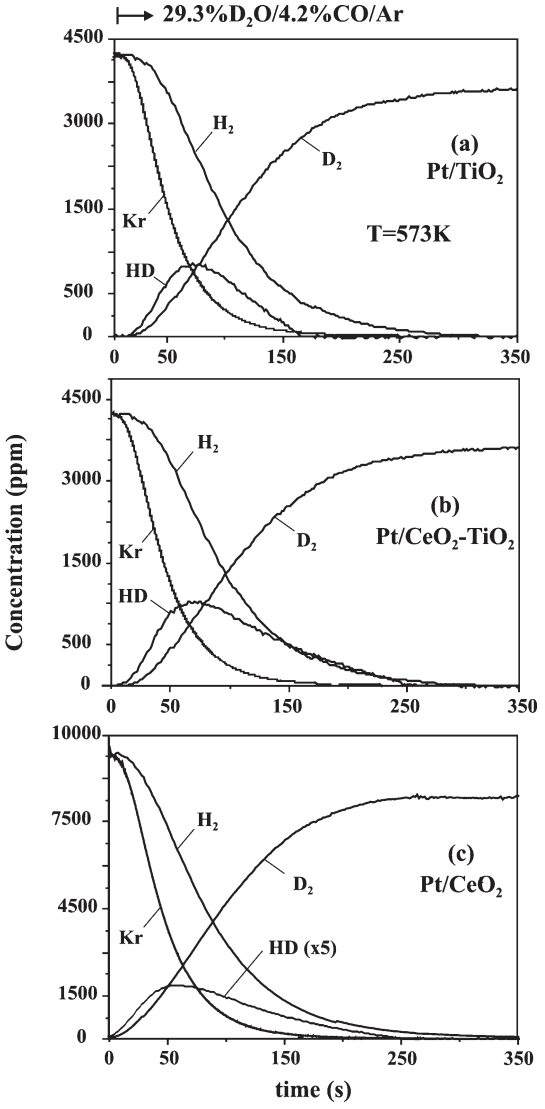

Figure 11. SSITKA−mass spectrometry experiments performed to estimate the concentration of active hydrogen-containing (H-pool) reaction intermediates found in the hydrogen path of WGS reaction on (a) Pt/TiO_2, (b) Pt/CeO_2-TiO_2, and (c) Pt/CeO_2 catalysts at 573 K. Gas delivery sequence: 4.2 vol % CO/29.3 vol % H_2O/Ar/Kr (30 min) → 4.2 vol % CO/29.3 vol % D_2O/Ar (t).

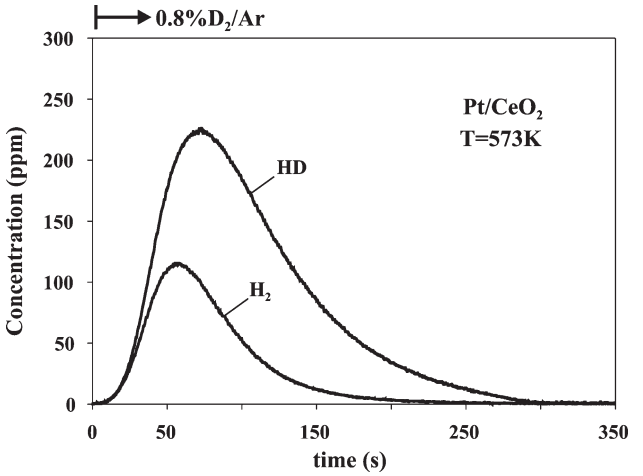

Figure 12. Transient isothermal (T = 573 K) concentration response curves of HD and H_2 gases recorded according to the following gas delivery sequence: 30 vol % H_2O/Ar (573 K, 30 min) → Ar (573 K, 10 min) → 0.8 vol % D_2/Ar (573 K, t) over a 0.5 wt % Pt/CeO_2 catalyst. W_{cat} = 0.025 g; F = 100 N mL/min.

around each Pt metal particle within which active OH/H species are formed and participate in the H-path of the WGS.

As the temperature of reaction increases to 573 K, the size of this active H-pool increases significantly ($172 < \theta_H < 225$, Table 2). Even in the case that formate is considered the main active carbon-containing intermediate at 573 K, the largest concentration of it can only be equivalent to $\theta = 7.2$ (Table 2), strongly indicating that at 573 K a significantly larger concentration of OH/H species is formed on the ceria support which is energetically capable to participate in the H-path of the WGS reaction. At the highest reaction temperature of 573 K, the concentration of H-containing intermediates increases in the following order: $CeO_2-TiO_2 > CeO_2 > TiO_2$ (Table 2).

3.4.4. Normal Kinetic Isotopic Effect. The SSITKA results reported in Figure 11 show that the rate of D_2 formation in the $^{12}CO/D_2O$/Ar reaction mixture is lower than the corresponding rate of H_2 formation in the $^{12}CO/H_2O$/Ar gas mixture, implying the existence of a normal kinetic isotopic effect (NKIE). The rate of H_2 formation appears to be greater than that of D_2 formation by a factor of 1.15, 1.14, and 1.18 for Pt/TiO_2, Pt/CeO_2-TiO_2, and Pt/CeO_2, respectively. The NKIE is related to the energy of chemical bond(s) involved in the rate-determining step (RDS), which for the present WGS reaction could be considered one of the following steps: (i) water dissociation on support (redox mechanism), (ii) formate (HCOO) decomposition (associative mechanism), (iii) surface diffusion of H/OH species (breaking of O−H bonds), and (iv) recombination of two adjacent adsorbed H species on Pt to form H_2(g).

A NKIE was also reported for other supported-Pt catalysts.[18,59,60] Ricote et al.[49] proposed that the rate-determining step could be that of formate decomposition on Pt to yield CO_2, but in the present work formates cannot be considered as active intermediates at 473 K. It was reported that water promotes the rate of WGS reaction on Pt/CeO_2[61] by the formation of −OH groups adjacent to the formate active intermediate, thus "a reactant-promoted" mechanism was proposed. Also, Grabow et al.[62] have investigated the mechanism of WGS on Pt(111) via DFT, microkinetic modeling, and experiments. The authors have shown that water can act as a promoter, making the low-energy COOH + OH decomposition step more accessible kinetically. Thus, water dissociation might be considered as a RDS in the case of WGS at 573 K on the present Pt/CeO_2 and Pt/CeO_2-TiO_2 catalysts but also at 473 K for a redox mechanism. Surface diffusion of H species from the −OH sites toward the metal−support interface may also be considered as RDS of the present WGS reaction system at 473 K.

3.5. Prevailing Mechanism of WGS—The Effect of Support Composition and Reaction Temperature. The present work has demonstrated the strong influence of support chemical composition and reaction temperature (ca. 473−573 K) on the chemical composition and surface coverage of active intermediates found in the H-path and C-path of WGS, and also of *spectator* species over supported-Pt catalysts. As mentioned in the Introduction section, four mechanistic routes have been reported for the WGS reaction, and these are outlined in Scheme 1: (A) redox, (B) carbonate, (C) associative formate with −OH group regeneration, and (D) associative mechanism.[10,16,18,21,22,60,63−65] Below we discuss the applicability

dx.doi.org/10.1021/jp201773a |J. Phys. Chem. C XXXX, XXX, 000–000

Scheme 1. Proposed Water−Gas Shift Reaction Mechanistic Pathways over Supported-Pt Catalysts.[22,34,65]

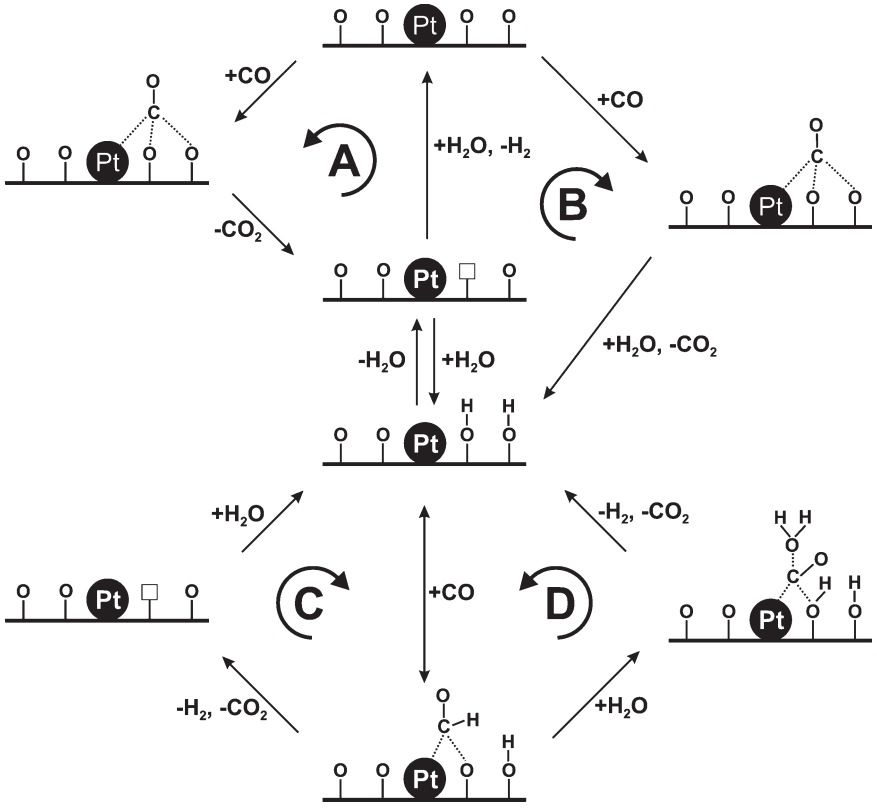

of these four mechanisms at 473 and 573 K over the three supported-Pt catalysts investigated.

3.5.1. Pt/CeO_2 Catalyst. As illustrated in Scheme 1A, adsorbed CO on a Pt site adjacent to an oxygen atom along the metal−support interface should be considered as an active species of the redox mechanism as supported by the works of Meunier et al.,[23,52,66] Bunluesin et al.,[8] and a recent work from our laboratory[22] for the WGS in the 523−573 K range. In fact, in the latter work the redox mechanism over Pt/CeO_2 (ceria sample was a commercial one of low surface area, ca. 5.6 $m^2 \cdot g^{-1}$, whereas Pt particle size was varied in the 1.3−8.0 nm range) was found to predominate over the associative formate with −OH group regeneration mechanism (Scheme 1C), the latter being considered to operate in parallel with the redox mechanism but contributing to a lesser extent in the overall WGS reaction rate. Many published works[44,61,65,67,68] have concluded that one of the two associative formate mechanisms (Scheme 1C or Scheme 1D) for the WGS operates on Pt/CeO_2. However, in all these studies no attempts were made to measure in situ the relative rates of WGS reaction at steady state or at the beginning of reaction (initial rates) associated with the assumed mechanism (e.g., redox versus associative formate) in order to provide strong support as to which mechanism prevails. The latter was performed successfully in recent works[22,23] by SSITKA−DRIFTS−MS and other transient isotopic experiments.

In Scheme 1D, formate intermediate decomposes to CO_2 through a surface carbonate intermediate in the presence of water (water-promoted dissociation of formate). This mechanism implies the presence of an active formate intermediate. However, the SSITKA−DRIFTS experiments showed that formate species is inactive at 473 K (Figure 3a). On the other hand, the carbonate mechanism (Scheme 1B) can be considered as a special case of the redox mechanism, since the main difference is the lifetime of the carbonate on the surface and the extent to which the two steps which involve reduction and reoxidation of support are separated in time.[38] For example, if both the decomposition of carbonate and reoxidation of support by water are fast steps, as occurs at high temperatures, the steady-state concentration of carbonate may be so small that it cannot be observed. As presented before, readsorption of CO_2 gas product to form surface carbonate species does occur, and an equilibrium condition (eq 7) is established under steady-state WGS. We have previously demonstrated[22] in a transient isotopic experiment that no reaction of preadsorbed carbonate species on Pt/CeO_2 at 573 K with adsorbed water did take place. Based on these findings, the carbonate route must be excluded.

Based on the above offered discussion, it can be concluded that the redox mechanism is the only one operating on Pt/CeO_2 at 473 K, whereas at 573 K the associative formate with −OH group regeneration mechanism also operates but to a lesser extent compared to the redox mechanism.[22] Formate species formed at 473 K under WGS is simply a spectator species. Meunier et al.[23,52,53,69] have recently applied an isotopic "operando" methodology on a 2 wt % Pt/CeO_2 catalyst where it was found that formate species was inactive at 433 K but became an active intermediate at 493 K, a behavior similar to that observed in the present 0.5 wt % Pt/CeO_2 and 0.5 wt % Pt/6.6 wt % CeO_2−TiO_2 catalysts.

3.5.2. Pt/TiO_2 Catalyst. According to the SSITKA−DRIFTS results of Figure 3c and 6c, the associative formate with −OH group regeneration (Scheme 1C) and associative (Scheme 1D) mechanisms which involve the formation of formate species must

dx.doi.org/10.1021/jp201773a |J. Phys. Chem. C XXXX, XXX, 000–000

be excluded at both WGS reaction temperatures. This is in harmony with our previous studies[21] performed on a different Pt/TiO_2 catalyst (different textural properties for the titania support, and similar Pt particle size), where the redox mechanism (Scheme 1A) was proved to better describe the experimental results obtained at 473 K. The carbonate mechanism (Scheme 1B) is also excluded by the fact that even though the red isotopic shift produced by carbonates was seen in the SSITKA−DRIFTS studies, the fact that chemisorption of CO_2 was proved to be reversible (see Figure 9) makes this route less possible especially at 473 K, where dehydroxylation or reduction of titania support by H_2 is required. We have performed a TPD experiment in He flow (use of mass spectrometry as detector) where the present Pt/TiO_2 catalyst was first treated in 30 vol % H_2O/He at 473 or 573 K for 1 h, followed by He purge to 303 K before TPD. No formation of gaseous H_2O was observed below 623 K. Thus, the rate of dehydroxylation depicted in Scheme 1B is insignificant below 573 K. Also, a H_2-TPR experiment (1 vol % H_2/He) performed on the preoxidized (773 K, 1 h, 20% O_2/He) Pt/TiO_2 catalyst resulted in two H_2-TPR traces, one below 553 K and the other one in the 563−873 K range, in very good agreement with the H_2-TPR traces reported[57] on a series of 0.5 wt % Pt/TiO_2 solids of different mean crystallite sizes for titania (16−35 nm). The rate of reduction at 573 K was estimated to be significantly lower than the WGS reaction rate at 573 K. These results suggest that reduction of titania under the present SSITKA−MS WGS experimental reaction conditions is not significant. We have also reported[21] that the presence of H_2 under WGS reaction conditions inhibits reoxidation of partially reduced titania. Based on all the above evidence, the carbonate route (Scheme 1B) is not favorable also on Pt/TiO_2.

3.5.3. Pt/CeO_2-TiO_2 Catalyst. According to the SSITKA−DRIFTS results of Figures 3b and 4b, this catalytic system follows the same characteristics regarding the nature of active reaction intermediates and inactive species formed as those of Pt/CeO_2 and Pt/TiO_2 catalysts. Thus, the redox mechanism is the only one operating under WGS at the low-T of 473 K. On the other hand, at the high-T of 573 K, the catalyst follows the characteristics of Pt/CeO_2 (see section 3.5.1); thus, the redox mechanism prevails over the associative formate with −OH group regeneration mechanism.

3.6. Volcano-type Activity Profile over Pt/TiO_2. The activity results depicted in Figure 1 show the formation of maximum activity at 548 K for the Pt/TiO_2 catalyst under the examined feed gas composition. The loss of activity at $T > 548$ K indicates that some changes occurred in catalyst's structure and/or in the adsorbed phase composition, which resulted in the decrease of catalyst's activity. The SSITKA−DRIFTS experiments performed at 473 and 573 K showed no changes in the operating mechanism in this temperature range. Based on the size of the C-pool at 473 and 573 K (Table 2), it is clear that the titania support facilitates the population of an increased concentration of CO precursor species related to inactive formate and carbonate species, as discussed in a previous section. It should also be noted that at 573 K a carbonate band (Figure 7c, band 2) did not provide the red isotopic shift, strongly indicating that this carbonate species is inactive. Previous studies[33] indicated that deactivation of Pt/TiO_2 was not related to a sintering process of platinum particles under WGS reaction conditions but to an over-reduction of the titania support; the term over-reduction refers to the fact that reoxidation of support is not taking place. In earlier studies[70,71] it was proposed that over-reduction could provoke the strengthening of binding energy of carbonate species on the support surface, thus leading to an autopoisoning. It was also reported that carbonates adsorbed on the platinum surface or associated to Pt sites at the metal−support interface could influence Pt surface electronic properties and accessibility to active metal sites. We suggest that inactive carbonate and formate species, and likely changes in the electronic properties of platinum nanoparticles at the metal support interface, contribute to the over-reduction phenomenon associated with the loss of activity of Pt/TiO_2 at $T > 548$ K. In the case of Pt/CeO_2-TiO_2, addition of 6.6 wt % of cerium oxide was sufficient to avoid over-reduction of TiO_2 at high temperatures.

According to the SSITKA−DRIFTS and SSITKA−MS experimental results presented in Figures 2−8 and 11, and Table 2, the coverage by ceria of the 45% of titania surface resulted in a catalytic system that resembles that of Pt/CeO_2 in terms of the nature of active reaction intermediates but which exhibits significantly lower surface concentrations for the active species present in the C-path at 473 and 573 K, and in the H-path at 473 K. This result could be interpreted as due to the enhancement of site reactivity of the active species imposed by the presence of a Ce−O−Ti−O interface in contact with Pt nanoparticles. The latter is reasonable given the different electron density of oxygen anions in the Ce−O−Ti moiety compared to that in the Ce−O−Ce and Ti−O−Ti moieties. Furthermore, electron charge flow between the O of Ce−O−Ti and Pt is expected to be different as compared to that for CeO_2 and TiO_2 supports alone. The latter would influence the chemisorpive properties of CO, thus the rate of WGS via the prevailing redox mechanism (Scheme 1A).

4. CONCLUSIONS

The following conclusions can be derived based on the results of the present work:

- The mechanism of WGS on 0.5 wt % Pt (d_{Pt} = 1.8−2.0 nm) supported on CeO_2, TiO_2, and CeO_2-TiO_2 in the 473−573 K range, and at conditions of a large water concentration (∼30 vol %) and a H_2O/CO ratio of about 7, was found to depend on reaction temperature and support chemical composition.
- In the case of CeO_2 and 6.6 wt % CeO_2-TiO_2 supports of Pt nanoparticles, the prevailing mechanism is that of redox (Scheme 1A), with the mechanism of associative formate with −OH group regeneration (Scheme 1C) to operate in parallel with the redox mechanism but contributing to a lower extent in the overall WGS reaction rate.[22] On the contrary, TiO_2 support promotes only the redox mechanism.
- The main active reaction intermediates found in both the redox and associative formate with −OH group regeneration mechanisms are located within a reactive zone around the Pt nanoparticles (∼1.8−2.0 nm). Their concentration largely exceeds one surface monolayer based on the Pt surface. Inactive species are formed, and these were found to be two different kinds of formates and carbonates located on the support.
- The Pt/CeO_2 and Pt/CeO_2-TiO_2 solids did not show any loss of catalytic activity after increasing the temperature in the 473−603 K range, as opposed to the case of Pt/TiO_2 which presents maximum at around 560 K. The latter is due to the over-reduction of support existing phenomenon.

dx.doi.org/10.1021/jp201773a |J. Phys. Chem. C XXXX, XXX, 000–000

AUTHOR INFORMATION

Corresponding Author
*Tel. +357 22 892776; fax +357 22 892801; e-mail efstath@ucy.ac.cy.

ACKNOWLEDGMENT

The financial support of the Cyprus Research Promotion Foundation (PENEK/ENISX/0308/50), CAM (P2009/ENE-1743), MICINN (ENE 2010-21198-C04-01), and INTA is gratefully acknowledged.

REFERENCES

(1) Basagiannis, A. C.; Verykios, X. E. *Appl. Catal., A* **2006**, *308*, 182.
(2) Chernik, S.; French, R.; Feik, C.; Chornet, E. *Ind. Eng. Chem. Res.* **2002**, *41*, 4209.
(3) Cortright, R. D.; Davda, R. R.; Dumesic, J. A. *Nature* **2002**, *418*, 964.
(4) Fu, Q.; Saltsburg, H.; Flytzani-Stephanopoulos, M. *Science* **2003**, *301*, 935 and references therein.
(5) Ratnasamy, C.; Wagner, J. P. *Catal. Rev.* **2009**, *51*, 325.
(6) Jacobs, G.; Davis, B. H. *Catalysis* **2007**, *20*, 122.
(7) Farrauto, R.; Hwang, S.; Shore, L.; Ruettinger, W.; Lampert, J.; Giroux, T.; Liu, Y.; Ilinich, O. *Annu. Rev. Mater. Res.* **2003**, *33*, 1.
(8) Bunluesin, T.; Gorte, R. J.; Graham, G. W. *Appl. Catal., B* **1998**, *15*, 107.
(9) Gorte, R. J.; Zhao, S. *Catal. Today* **2005**, *104*, 18.
(10) Hilaire, S.; Wang, X.; Luo, T.; Gorte, R. J.; Wagner, J. *Appl. Catal., A* **2001**, *215*, 271.
(11) Li, Y.; Fu, Q.; Flytzani-Stephanopoulos, M. *Appl. Catal., B* **2000**, *27*, 179.
(12) Liu, W.; Flytzani-Stephanopoulos, M. *J. Catal.* **1995**, *153*, 317.
(13) Silberova, B. A. A.; Mul, G.; Makkee, M.; Moulijn, J. A. *J. Catal.* **2006**, *243*, 171.
(14) Chenu, E.; Jacobs, G.; Crawford, A. C.; Keogh, R. A.; Patterson, P. M.; Sparks, D. E.; Davis, B. H. *Appl. Catal., B* **2005**, *59*, 45.
(15) Jacobs, G.; Graham, U. M.; Chenu, E.; Patterson, P. M.; Dozier, A.; Davis, B. H. *J. Catal.* **2005**, *229*, 499.
(16) Jacobs, G.; Williams, L.; Graham, U.; Sparks, D.; Davis, B. H. *J. Phys. Chem. B* **2003**, *107*, 10398.
(17) Jacobs, G.; Williams, L.; Graham, U.; Thomas, G. A.; Sparks, D. E.; Davis, B. H. *Appl. Catal., A* **2003**, *252*, 107.
(18) Shido, T.; Iwasawa, Y. *J. Catal.* **1993**, *141*, 71 and references therein.
(19) Zhai, Y.; Pierre, D.; Si, R.; Deng, W.; Ferrin, P.; Nilekar, A. U.; Peng, G.; Herron, J. A.; Bell, D. C.; Saltsburg, H.; Mavrikakis, M.; Flytzani-Stephanopoulos, M. *Science* **2010**, *329*, 1633 and references therein.
(20) Rodriguez, J. A.; Ma, S.; Liu, P.; Hrbek, J.; Evans, J.; Pérez, M. *Science* **2007**, *318*, 1757.
(21) Kalamaras, C. M.; Panagiotopoulou, P.; Kondarides, D. I.; Efstathiou, A. M. *J. Catal.* **2009**, *264*, 117 and references therein.
(22) Kalamaras, C. M.; Americanou, S.; Efstathiou, A. M. *J. Catal.* **2011**, *279*, 287.
(23) Meunier, F. C. *Catal. Today* **2010**, *155*, 164.
(24) Efstathiou, A. M.; Verykios, X. E. *Appl. Catal., A* **1997**, *151*, 109.
(25) Kundakovic, L.; Flytzani-Stephanopoulos, M. *J. Catal.* **1998**, *179*, 203.
(26) Zhu, H.; Shen, M.; Kong, Y.; Hong, J.; Hu, Y.; Lin, T.; Dong, L.; Chen, Y.; Jian, C.; Liu, Z. *J. Mol. Catal. A: Chem.* **2004**, *219*, 155.
(27) Ojeda, M.; Granados, M. L.; Rojas, S.; Terreros, P.; García-García, F. J.; Fierro, J. L. G. *Appl. Catal., A* **2004**, *261*, 47.
(28) Pedrero, C.; Waku, T.; Iglesia, E. *J. Catal.* **2005**, *233*, 242.
(29) Patterson, A. L. *Phys. Rev.* **1939**, *56*, 978.
(30) Polychronopoulou, K.; Costa, C. N.; Efstathiou, A. M. *Appl. Catal., A* **2004**, *272*, 37.
(31) Kalamaras, C. M.; Olympiou, G. G.; Efstathiou, A. M. *Catal. Today* **2008**, *138*, 228.
(32) Olympiou, G. G.; Kalamaras, C. M.; Zeinalipour-Yazdi, C. D.; Efstathiou, A. M. *Catal. Today* **2007**, *127*, 304.
(33) González, I. D.; Navarro, R. M.; Wen, W.; Marinkovic, N.; Rodriguéz, J. A.; Rosa, F.; Fierro, J. L. G. *Catal. Today* **2010**, *149*, 372.
(34) Jacobs, G.; Davis, B. H. *Appl. Catal., A* **2007**, *333*, 192.
(35) Panagiotopoulou, P.; Kondarides, D. I. *Appl. Catal., B* **2011**, *101*, 738.
(36) Panagiotopoulou, P.; Kondarides, D. I. *Catal. Today* **2006**, *112*, 49.
(37) Panagiotopoulou, P.; Kondarides, D. I. *J. Catal.* **2004**, *225*, 327.
(38) Burch, R. *Phys. Chem. Chem. Phys.* **2006**, *8*, 5483.
(39) Panagiotopoulou, P.; Papavasiliou, J.; Avgouropoulos, G.; Ioannides, T.; Kondarides, D. I. *Chem. Eng. J.* **2007**, *134*, 16.
(40) Li, C.; Sakata, Y.; Arai, T.; Domen, K.; Maruya, K.-I.; Onishi, T. *J. Chem. Soc., Faraday Trans. 1* **1989**, *85*, 929.
(41) Bazin, P.; Saur, O.; Lavalley, J. C.; Daturi, M.; Blanchard, G. *Phys. Chem. Chem. Phys.* **2005**, *7*, 187.
(42) Azzam, K. G.; Babich, I. V.; Seshan, K.; Lefferts, L. *J. Catal.* **2007**, *251*, 153.
(43) Jacobs, G.; Patterson, P. M.; Graham, U. M.; Sparks, D. E.; Davis, B. H. *Appl. Catal., A* **2004**, *269*, 63.
(44) Jacobs, G.; Patterson, P. M.; Williams, L.; Chenu, E.; Sparks, D.; Thomas, G.; Davis, B. H. *Appl. Catal., A* **2004**, *262*, 177.
(45) Jacobs, G.; Ricote, S.; Davis, B. H. *Appl. Catal., A* **2005**, *284*, 31.
(46) Jacobs, G.; Ricote, S.; Davis, B. H. *Appl. Catal., A* **2006**, *302*, 14.
(47) Li, C.; Sakata, Y.; Arai, T.; Domen, K.; Maruya, K.-I.; Onishi, T. *J. Chem. Soc., Faraday Trans. 1* **1989**, *85*, 1451.
(48) Martin, D.; Duprez, D. *J. Phys. Chem. B* **1997**, *101*, 4428.
(49) Ricote, S.; Jacobs, G.; Milling, M.; Ji, Y.; Patterson, P. M.; Davis, B. H. *Appl. Catal., A* **2006**, *303*, 35.
(50) Iida, H.; Igarashi, A. *Appl. Catal., A* **2006**, *303*, 48.
(51) Liao, L. F.; Lien, C. F.; Shieh, D. L.; Chen, M. T.; Lin, J. L. *J. Phys. Chem. B* **2002**, *106*, 11240.
(52) Meunier, F. C.; Tibiletti, D.; Goguet, A.; Shekhtman, S.; Hardacre, C.; Burch, R. *Catal. Today* **2007**, *126*, 143.
(53) Meunier, F. C.; Goguet, A.; Hardacre, C.; Burch, R.; Thompsett, D. *J. Catal.* **2007**, *252*, 18.
(54) Primet, M. *J. Catal.* **1984**, *88*, 273.
(55) Primet, M.; Basset, J. M.; Mathieu, M. V.; Prettre, M. *J. Catal.* **1973**, *29*, 213.
(56) Shannon, S. L.; Goodwin, J. G., Jr. *Chem. Rev.* **1995**, *95*, 677.
(57) Panagiotopoulou, P.; Christodoulakis, A.; Kondarides, D. I.; Boghosian, S. *J. Catal.* **2006**, *114*, 240.
(58) Tejuca, L. G.; Bell, A. T.; Fierro, J. L. G.; Peña, M. A. *Appl. Surf. Sci.* **1988**, *31*, 301.
(59) Jacobs, G.; Crawford, A.; Williams, L.; Patterson, P. M.; Davis, B. H. *Appl. Catal., A* **2004**, *267*, 27.
(60) Shido, T.; Iwasawa, Y. *J. Catal.* **1992**, *136*, 493.
(61) Jacobs, G.; Davis, B. H. *Int. J. Hydrogen Energy* **2010**, *35*, 3522.
(62) Grabow, L. C.; Gokhale, A. A.; Evans, S. T.; Dumesic, J. A.; Mavrikakis, M. *J. Phys. Chem. C* **2008**, *112*, 4608.
(63) Fu, Q.; Weber, A.; Flytzani-Stephanopoulos, M. *Catal. Lett.* **2001**, *77*, 87.
(64) Mhadeshwar, A. B.; Vlachos, D. G. *J. Phys. Chem. B* **2004**, *108*, 15246.
(65) Azzam, K. G.; Babich, I. V.; Seshan, K.; Lefferts, L. *J. Catal.* **2007**, *251*, 153.
(66) Meunier, F. C.; Reid, D.; Goguet, A.; Shekhtman, S.; Hardacre, C.; Burch, R.; Deng, W.; Flytzani-Stephanopoulos, M. *J. Catal.* **2007**, *247*, 277.
(67) Jacobs, G.; Khalid, S.; Patterson, P. M.; Sparks, D. E.; Davis, B. H. *Appl. Catal., A* **2004**, *268*, 255.
(68) Jacobs, G.; Crawford, A. C.; Davis, B. H. *Catal. Lett.* **2005**, *100*, 147.

(69) Meunier, F. C.; Tibiletti, D.; Goguet, A.; Burch, R. *Oil Gas Sci. Technol.* **2006**, *61*, 497.
(70) Goguet, A.; Meunier, F. C.; Tibiletti, D.; Breen, J. P.; Burch, R. *J. Phys. Chem. B* **2004**, *108*, 20240.
(71) Liu, X. S.; Ruettinger, W.; Xu, X. M.; Farrauto, R. *Appl. Catal., B* **2005**, *56*, 69.